Three-dimensional bipedal model with zero-energy-cost walking

Sergey Pankov [*]

Harik Shazeer Labs, Palo Alto, California 94301, USA

We study a three-dimensional articulated rigid-body biped model that possesses zero cost of transport walking gaits. Energy losses are avoided due to the complete elimination of the foot-ground collisions by the concerted oscillatory motion of the model's parts. The model consists of two parts connected via a universal joint. It does not rely on any geometry-altering mechanisms, massless parts, or springs. Despite the model's simplicity, its collisionless gaits feature walking with finite speed, foot clearance, and ground friction. The collisionless spectrum can be studied analytically in the small movement limit, revealing infinitely many periodic modes. The modes differ in the number of sagittal and coronal plane oscillations at different stages of the walking cycle. We focus on the mode with the minimal number of such oscillations, presenting its complete analytical solution. We then numerically evolve it toward a general nonsmall movement solution. A general collisionless mode can be tuned by adjusting a single model parameter. Some of the presented results display a surprising degree of generality and universality.

I. INTRODUCTION

Arguably, energy efficiency is one of the two most important issues in the field of robotic locomotion [1] (the other one—control robustness—is outside the scope of this paper). Efficiency makes an autonomous robot proportionally more useful, as it can run longer on a single power refill [2] (e.g., battery charge) and wears out its hardware more slowly. A common measure of efficiency for mobile robots is the cost of transport (COT)—the amount of energy spent by a traveling robot per its weight per distance traveled.

The importance of energy efficiency is not limited to man-made machines. As it offers a clear survival advantage, it is natural to expect for animal gaits to be significantly shaped by the energy efficiency requirements [3]. Indeed, optimizing a detailed human neuromusculoskeletal model for COT produces a gait similar to a natural human gait [4].

Likewise, when anthropomorphic robots are designed with COT optimality as the main objective, their walking gaits often appear humanlike [5,6]. Walking motion patterns in these robots are mostly decided by their passive dynamics. To sustain walking, they need a relatively small energy injection, either through joint actuation or by walking on a slight incline.

Since COT optimality plays a prominent role, it is reasonable to ask how energy is lost during walking and how these losses can be minimized. In this paper, we are only concerned with mechanical losses. In general, energy is lost when the robot's actuators work against its passive dynamics and when its feet interact with the ground. For a passive walker, only the latter is of concern: energy is lost when a foot either collides with or slides against the ground. To avoid the collision loss, the foot velocity must vanish at the contact. For the foot then

to stay on the ground, its acceleration must also vanish [7], while the jerk (time derivative of acceleration) should remain finite at the contact [8]. This type of collisionless motion has been proposed and demonstrated in a hopper [7,8] and a rimless wheel [9,10].

Note, if only velocity vanishes at the contact [11], an additional mechanism (e.g., suction cups) is needed to keep the robot in contact with the surface, as the surface reaction force is negative (directed into the surface away from the robot) when the contact occurs, as in brachiation [12]. If the ground reaction force is non-negative everywhere on a walking trajectory, we call such walking conventional.

For an appropriately designed walker, the collision losses can be made to scale as the fourth power of velocity [13], thereby COT vanishes as the third power at low velocity. From a certain practical stand point, such elimination of COT in the limit may be of limited utility. In this paper, we are concerned with finding a finite-speed collisionless solution. We are also not interested in nonphysical solutions, such as considering massless springs, even though they trivially provide for a lossless locomotion.

Some passive walker models require additional active mechanisms to practically realize their walking modes. For example, leg retraction may be needed to prevent ground scuffing [13] or knees may need to be actively locked for a portion of a walking cycle [14]. While technically realizable, they add to the engineering challenge [15] and ideally should be avoided, if possible.

In this paper, we report a three-dimensional passive walker model with a perfectly collisionless finite-speed walking gait. The model is free of nuisances requiring engineering intervention. The ground scuffing is avoided by a rocking motion in the coronal plane, without altering the model's geometry. There is no joint locking. The robot is made of articulated rigid parts without use of springs. The walking gait is

---

[*]sergey.pankov@gmail.com

realized at finite ground friction. The existence of a collision-less solution is demonstrated analytically. To date, to the best of our knowledge, no collissionless finite-speed conventional bipedal walking in a physically realistic model has been con-clusively demonstrated by solving equations of motion, either numerically or analytically, in either two or three dimensions.

The analytical solution is obtained via a perturbation the-ory in the feet separation parameter, to the lowest order necessary to establish a nontrivial (i.e., walking) collisionless solution. This amounts to considering the sagittal and coronal dynamics to linear order and the axial dynamics to quadratic order. The perturbative treatment is justified under certain conditions, which we collectively term the small movement limit (SML). A SML solution can be numerically evolved to a general solution using constrained gradient descent optimization.

We showed that the number of model parameters needed for tuning a collisionless solution is in general independent of the model complexity and only depends on the topological properties of the foot-ground interaction. Interestingly, our SML solution is to a significant degree encoded by a pair of universal functions, completely independent of the model parametrization. It is an intriguing possibility that this univer-sality of the collisionless solution is not coincidental to our model but may be generalizable to other models as well.

The solution of our springless model features a peculiar hanging torso gait. To enable a more-anthropomorphic look-ing standing torso gait, we also considered a model endowed with springs. We established an up-down torso duality and exploited it to formulate the standing torso solution in terms of the original springless model solution.

The paper is organized as follows. The biped model is introduced in Sec. II. In Sec. III, we derive the exact equa-tions of motion, as well as their approximate and simpler SML form. Certain symmetry constraints are imposed on the general solution in Sec. IV to make the solution search more manageable. The SML solution is analytically investigated throughout Sec. V. The found SML solution is employed as an initial guess for a general numerical solution presented in Sec. VI. In Sec. VII, we discuss related work and outline directions for possible future research. Throughout this paper, for the sake of both clarity and completeness of presentation, many technical details have been relegated to the Appendices.

II. MODEL, TERMINOLOGY, AND NOTATIONS

In this section, we introduce the biped model, related ter-minology, and some ubiquitous notations.

The biped model is depicted in Fig. 1. It is composed of two rigid parts, called legs and torso, connected at the hip via a universal joint. The endpoints of the legs coming in contact with the ground ($z = 0$ plane) are called feet. The hip and feet form an isosceles triangle (with the hip at the apex). In the figure, the biped is shown in the upright configuration, char-acterized by the reflection symmetries relative to the coronal ($x = 0$) and sagittal ($y = 0$) planes.

We limit our consideration to periodic walking motion. Walking consists of alternating single and double support phases. In the double support phase, called phase II, both feet are on the ground. In the single support phase, called phase I,
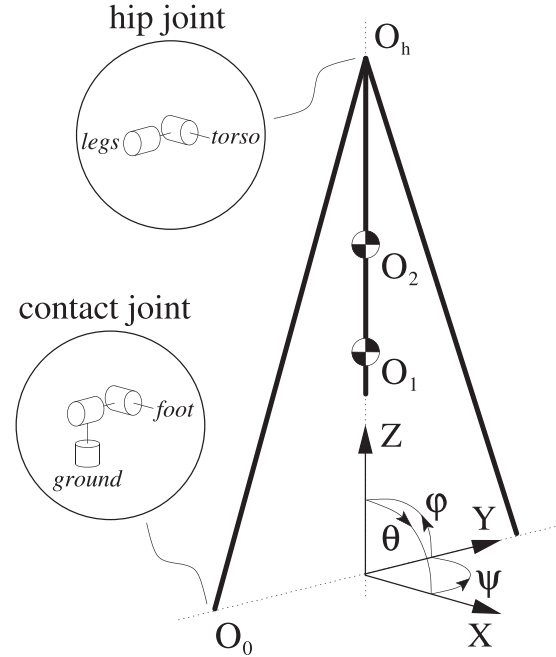

FIG. 1. Biped model. The figure is schematic: In general, the depicted leg and torso links should not be regarded as indicative of the mass distribution.

only one foot (called stance foot) is on the ground. The other foot (called swing foot) is moved to a new location during phase I, thereby realizing a stepping motion.

Unless stated otherwise, by collisionless walking (gait or solution) we mean collisionless conventional walking, that is, with both velocity and acceleration vanishing at the moment of contact. Because a collisionless gait conserves energy, it is time reversible. Therefore, we do not need to distinguish between a foot strike and liftoff. We refer to both as an impact event, foot impact, or impact for short.

Before we proceed, a few words are in order about our matrix conventions. We use square brackets to denote a ma-trix, commas to separate matrix elements, and semicolons to separate matrix rows. Vectors are in column format. Due to heavy use of sub- and superscripts, we use parentheses to explicitly indicate vector or matrix component indices, unless noted otherwise. A component index can be replaced by the dot symbol to select all elements it represents. For example, $M_{(i\cdot)}$ and $M_{(\cdot j)}$ are ith row and jth column of a matrix M. Transposition is denoted $M^{\mathsf{T}}_{(ij)} = M_{(ji)}$. The Kronecker delta is $\delta_{ij} \equiv \delta_{(ij)}$. An identity matrix $I_{n \times m}$ is $n \times m$ matrix $I_{n \times m (ij)} = \delta_{ij}$; also, $I \equiv I_{3 \times 3}$.

The contact of the stance foot can be modeled as a fictitious spherical joint attaching the biped to the ground. The universal and spherical joints can be viewed as two and three hinge joints respectively, connected in series, see Fig. 1. We use ϕ, θ, and ψ to denote rotation angles in the coronal, sagittal, and axial ($z = 0$) planes, correspondingly. In phase I, hinge angles $q_t^s = [\phi_t, \theta_t]^{\mathsf{T}}$ specify the torso's orientation relative to the legs, and hinge angles $q_l^s = [\phi_l, \theta_l, \psi_l]^{\mathsf{T}}$ specify the legs' orientation relative to the ground. In phase II, the degrees ϕ_l and ψ_l are inactive, therefore $q_l^d = [\theta_l]$, while $q_t^d = q_t^s$. The model's configuration is fully specified by the generalized co-

ordinates $q^p = [q_l^p; q_t^p]$, where the support phase superscript p stands for s and d in the single and double support phases, respectively. In the upright configuration $q_{(i\neq3)}^s = 0$ by convention. We will also refer to $q_\phi = [\phi_l, \phi_t]^\mathsf{T}$, $q_\theta = [\theta_l, \theta_t]^\mathsf{T}$, and ψ_l subspaces as the coronal (or ϕ), sagittal (or θ), and axial (or ψ) sectors, correspondingly.

It is often convenient to work in a body-fixed frame of a rigid body. Let us denote the ground frame, the legs' body frame, and the torso's body frame as F_g, F_l, and F_t, correspondingly. The ground frame F_g is shown in Fig. 1. By convention, in the upright configuration, $F_g = F_l = F_t$. In general, for vectors and matrices we may optionally use the frame superscript (g, l, or t) to explicitly indicate the frame their components are written in. For many quantities, we can omit the frame superscript (unless expressly stated otherwise) when we are not concerned with a coordinate representation or when the ground frame is implied. The rotation matrix R_{ab} rotates vector coordinates from F_a to F_b, that is, $r^a = R_{ab}r^b$ for a vector r. The angular velocity of F_b relative to F_a is $\hat\Omega_{ab} = \dot{R}_{ab}R_{ab}^\mathsf{T}$, where the hat notation indicates a skew symmetric matrix $\hat{a}$ defined via the antisymmetric symbol as $\hat{a}_{(ij)} = \sum_k \epsilon_{(jik)}a_{(k)}$. For convenience, we may introduce shorthand notations. For example, we define $R_1 \equiv R_{gl}$, $R_t \equiv R_{lt}$, $\Omega_1 \equiv \Omega_{gl}$, $\Omega_t \equiv \Omega_{lt}$, and $\Omega_2 \equiv \Omega_{gt} = \Omega_1 + \Omega_t$. The precise specifications of the joints' parametrization and hence the dependence of R and Ω on q and $\dot{q}$ are presented in Appendix A.

The model's geometric and inertial parameters are specified as follows. Let O_0, O_1, O_2, and O_h be the foot, the legs' center of mass (COM), the torso's COM, and the hip, respectively, as shown in Fig. 1. We define $r_1 = \overrightarrow{O_0O_1}$, $r_2 = \overrightarrow{O_0O_2}$, $r_h = \overrightarrow{O_0O_h}$, and $r_t = \overrightarrow{O_hO_2}$. Note r_1^l, r_h^l, and r_t^t are constants, defined by the following parametrization:

$$r_1^l = \begin{bmatrix} 0 \\ d \\ l_1 \end{bmatrix}, \quad r_h^l = \begin{bmatrix} 0 \\ d \\ l_h \end{bmatrix}, \quad r_t^t = \begin{bmatrix} 0 \\ 0 \\ -l_t \end{bmatrix}. \quad (1)$$

At the upright configuration, $r_2 = r_h + r_t = [0, d, l_2]$, where $l_2 = l_h - l_t$. In many cases, such as for COM's location r_i, mass m_i, and the moment of inertia I_i, we use $i = 1$ and $i = 2$ to designate the parameters of the legs and torso, respectively. The stated model symmetries (reflections in the sagittal and coronal planes) imply that I_i are diagonal in the respective body frames: $I_1^l = \mathrm{diag}(I_{1\phi}, I_{1\theta}, I_{1\psi})$ and $I_2^t = \mathrm{diag}(I_{2\phi}, I_{2\theta}, I_{2\psi})$.

Let us define a mass distribution moment function:

$$\mu_{na} = m_1 l_1^n + m_2 l_a^n. \quad (2)$$

We will often be using the following shorthand notations: $\mu_n \equiv \mu_{n2}$, $\tilde\mu_n \equiv \mu_{nh}$ and $I_\alpha \equiv I_{1\alpha} + I_{2\alpha}$.

III. EQUATIONS OF MOTION

In this section, we first derive the exact equations of motion. These equations can only be integrated numerically. We next derive the SML equations—an approximation to the exact equations—that we analyze and solve analytically later on in Sec. V. When solving numerically for a general collisionless solution, we will use the SML solution as an initial guess, which can be very helpful in a numerical solution search.

A. Exact equations

The kinetic and potential energies, written in terms of the model part coordinates and velocities, are

$$T = \frac{1}{2} \sum_{i=1,2} \left(m_i v_i^\mathsf{T} v_i + \Omega_i^\mathsf{T} I_i \Omega_i \right),$$
$$V = -g_f^\mathsf{T} \sum_{i=1,2} m_i r_i, \quad (3)$$

where m_i are masses, I_i are moments of inertia, r_i are COM coordinates, v_i are COM velocities, Ω_i are angular velocities, and $g_f = [0, 0, -g]^\mathsf{T}$ is the gravitational field vector. The legs and torso parameters are indicated by $i = 1$ and $i = 2$, correspondingly. Following the Lagrangian formalism to derive the equations of motion [16,17], we need to express T and V in terms of the generalized coordinates q and velocities $\dot{q}$, define the Lagrangian function $\mathcal{L}(q, \dot{q}) = T(q, \dot{q}) - V(q)$, and write down the Euler-Lagrange equations:

$$\frac{d}{dt}\frac{\partial \mathcal{L}}{\partial \dot{q}} - \frac{\partial \mathcal{L}}{\partial q} = 0. \quad (4)$$

We first consider phase I, so we assume below $q = q^s$. The kinetic energy can be written in the form $T = \frac{1}{2}\dot{q}^\mathsf{T} H \dot{q}$, where H is called the mass matrix. It can be written as

$$H = \bar{S}^\mathsf{T} \bar{H} \bar{S}, \quad (5)$$

where $\bar{S}$ is constructed from the joint rotations R_1 and R_t (and corresponding partial rotations) and $\bar{H}$ is expressed in terms of the model constants (r_1^l, r_h^l, r_t^t, m_1, m_2, I_1^l, I_2^t) and R_t, see Appendix B for details. Specifically, for $\bar{S}$ we have

$$\bar{S} = \begin{bmatrix} R_1^\mathsf{T} S_1 & 0 \\ 0 & R_t^\mathsf{T} S_t \end{bmatrix} = \begin{bmatrix} S_1^l & 0 \\ 0 & S_t^t \end{bmatrix}, \quad (6)$$

where

$$S_1 = [(R_Z(\psi_l)R_Y(\theta_l))_{(\cdot1)}, R_Z(\psi_l)_{(\cdot2)}, I_{(\cdot3)}] \quad (7)$$

and

$$S_t = [R_Y(\theta_t)_{(\cdot1)}, I_{(\cdot2)}]. \quad (8)$$

For $\bar{H}$, we have

$$\bar{H} = \begin{bmatrix} \bar{H}_{ll} & \bar{H}_{lt} \\ \bar{H}_{tl} & \bar{H}_{tt} \end{bmatrix}, \quad (9)$$

where

$$\bar{H}_{ll} = m_1 \widehat{r_1^l}^\mathsf{T} \widehat{r_1^l} + I_1^l + R_t(m_2 \widehat{r_2^t}^\mathsf{T} \widehat{r_2^t} + I_2^t)R_t^\mathsf{T},$$
$$\bar{H}_{lt} = \bar{H}_{tl}^\mathsf{T} = R_t(m_2 \widehat{r_2^t}^\mathsf{T} \widehat{r_t^t} + I_2^t), \quad (10)$$
$$\bar{H}_{tt} = m_2 \widehat{r_t^t}^\mathsf{T} \widehat{r_t^t} + I_2^t,$$

where $\widehat{r_2^t} = \widehat{R_t^\mathsf{T} r_h^l} + \widehat{r_t^t}$.

Following the standard procedure [17], we use the mass matrix H to define the Coriolis matrix C in terms of the Christoffel symbols $\Gamma_{(ijk)}$ as

$$C = \sum_k \Gamma^k \dot{q}_{(k)}, \quad (11)$$

where

$$\Gamma_{(ij)}^k = \Gamma_{(ijk)} = \frac{1}{2}\left(\frac{\partial H_{(ij)}}{\partial q_{(k)}} + \frac{\partial H_{(ik)}}{\partial q_{(j)}} - \frac{\partial H_{(jk)}}{\partial q_{(i)}} \right). \quad (12)$$

The potential energy, written explicitly in terms of the model constants and joint rotations, is

$$V = g\big(R_1\big(m_1 r_1^l + m_2\big(r_h^l + R_t r_t^t\big)\big)\big)_{(3)}, \quad (13)$$

where g is the gravity acceleration magnitude. The potential term G is defined as the gradient of the potential energy $V(q)$

$$G = \nabla V. \quad (14)$$

We are now in a position to write down the equations of motion in the manipulator equation form [17],

$$H\ddot{q} + C\dot{q} + G = 0, \quad (15)$$

where H, C, and G have been defined above. These terms are defined explicitly in terms of the model parameters, save for differentiation with respect to q, which can be done either symbolically (manually or with help of differentiation software) or numerically. The equation can then be integrated numerically.

We next consider phase II. The leg coordinates q_l change from $[\phi_l, \theta_l, \psi_l]^{\mathsf{T}}$ in phase I to $[\theta_l]$ in phase II. Correspondingly, R_1 becomes $R_Y(\theta_l)$ and S_1 becomes $I_{(\cdot2)}$. The equations of motion in phase II can be formally written as a projection of the phase-I equations. To that end, we introduce a projection operator J^d that projects q^s onto q^d: $q^d = J^d q^s$. It is defined as $J^d_{(1,2)} = J^d_{(2,4)} = J^d_{(3,5)} = 1$ with all other entrees equal to zero. We also define a projection operator $J^s = J^{d\mathsf{T}} J^d$, which zeros out q^s components that are absent in q^d, namely, $q^s_{(1)}$ and $q^s_{(3)}$. The phase I Eq. (15) can be written as $D^s q = 0$, where $D^s(q, \dot{q}) = H(q)\frac{d^2}{dt^2} + C(q, \dot{q})\frac{d}{dt} + \|q\|^{-2}G(q)q^{\mathsf{T}}$. The phase-II equations of motion $D^d q^d = 0$ can then be obtained by projecting

$$D^d = J^d D^s (J^s q, J^s \dot{q}) J^{d\mathsf{T}}. \quad (16)$$

We next consider the equations of motion in the SML approximation.

B. Small movement limit

The SML is essentially a relationship between relevant problem scales in the limit of small feet separation that justifies perturbation theory treatment in which the dynamics of the ψ sector are decided at higher order by the (decoupled at lower order) ϕ and θ sectors. To specify it precisely, we introduce dimensionless parameters: dimensionless foot separation parameter $\bar{d} = \mu_0 d/\mu_1$ and dimensionless axial moment of inertia $\bar{I}_\psi = I_\psi/\mu_2$. We will see in this section that $\phi \sim \bar{d}$, $\theta \sim \varepsilon$ and $\psi \sim \bar{d}\varepsilon/\bar{I}_\psi$, where ε is a free scale parameter, independent of the model parametrization. For the consistency of our perturbative analysis, we need $1 \gg \phi, \theta \gg \psi, \phi^2, \theta^2$, from where we obtain the SML specifications:

$$\text{SML}: \begin{cases} \bar{d} \ll 1 \\ \bar{d}^2 \ll \varepsilon \ll \sqrt{\bar{d}} \\ \bar{I}_\psi \gg \max\{\bar{d}, \varepsilon\}. \end{cases} \quad (17)$$

A more careful analysis reveals that these conditions can be relaxed somewhat (e.g., the third line can be replaced by $\bar{I}_\psi \gg \bar{d}^2$), but for the sake of simplicity we define the SML as above. Below we expand the exact equations of motion to the lowest order sufficient for establishing a nontrivial walking solution.

First we consider phase I. In the linear dynamics limit, the equations of motion are

$$H_0\ddot{q} + G_0 + G_1 q = 0, \quad (18)$$

where H_0, G_0, and G_1 are derived in Appendix C, (nonperturbatively in $\bar{d}$, i.e., correct to all orders in $\bar{d}$). In this limit, the ϕ sector is completely decoupled from the other sectors. The θ sector is coupled to the ψ sector via $O(\bar{d})$ coupling. To the lowest nontrivial order in $\bar{d}$, (namely, to order $O(1)$ for H_0 and G_1, and to order $O(\bar{d})$ for G_0, which coincidentally are exact expressions for G_0 and G_1), the equations of motion in $\alpha \in \{\phi, \theta\}$ sectors assume a similar form:

$$H_\alpha = \begin{bmatrix} \mu_2 + I_\alpha & -m_2 l_2 l_t + I_{2\alpha} \\ -m_2 l_2 l_t + I_{2\alpha} & m_2 l_t^2 + I_{2\alpha} \end{bmatrix},$$
$$G_{0\alpha} = g\begin{bmatrix} \delta_{\alpha\phi}\mu_0 d \\ 0 \end{bmatrix}, \quad G_{1\alpha} = g\begin{bmatrix} -\mu_1 & m_2 l_t \\ m_2 l_t & m_2 l_t \end{bmatrix}. \quad (19)$$

Note $G_{0\phi}$ is $O(\bar{d})$, while $G_{0\theta} = 0$. As a consequence, the scale of ϕ sector motion is controlled by $\bar{d}$, while the scale ε of θ sector motion is not determined by the model parameters, but only needs to be $\varepsilon \ll 1$ to justify the linear dynamics approximation.

To the considered order [as in Eqs. (19)], $\ddot{\psi}_l = 0$ and the solution describes a walking-in-place motion (walking with zero step size). To capture a nontrivial motion in the ψ sector, we need to include the terms to order $O(\bar{d}\varepsilon)$ in the equations of motion, for the purpose of computing ψ_l. This entails including the terms of order $O(\bar{d})$ from H_0, as well as the order $O(q)$ corrections to the mass matrix H and Coriolis term C, see Appendix D for details. The equations of motion for ψ_l in the SML become

$$I_\psi \ddot{\psi}_l + d b^{\mathsf{T}} \ddot{q}_\theta + \frac{d}{dt}\big(q_\phi^{\mathsf{T}} A_{\phi\theta} \dot{q}_\theta + q_\theta^{\mathsf{T}} A_{\theta\phi} \dot{q}_\phi\big) = 0, \quad (20)$$

where

$$b = \begin{bmatrix} -\mu_1 \\ m_2 l_t \end{bmatrix} \quad (21)$$

and

$$A_{\phi\theta} = \begin{bmatrix} \mu_2 + I_\theta - I_\psi & -m_2 l_2 l_t + I_{2\theta} \\ -m_2 l_2 l_t + I_{2\theta} - I_{2\psi} & m_2 l_t^2 + I_{2\theta} - I_{2\psi} \end{bmatrix},$$
$$A_{\theta\phi} = \begin{bmatrix} -\mu_2 - I_\phi & m_2 l_2 l_t - I_{2\phi} \\ m_2 l_2 l_t - I_{2\phi} + I_{2\psi} & -m_2 l_t^2 \end{bmatrix}. \quad (22)$$

These equations properly account for all the dominant terms up to $O(\bar{d}\varepsilon)$, as long as the SML conditions of Eq. (17) are satisfied.

In the SML, rather than working with relative angles (joint angles) as generalized coordinates in $\alpha \in \{\phi, \theta\}$ sectors, we found it convenient to work with absolute angles measured with respect to the statically balanced single support configuration. (G becomes diagonal in that basis.) Therefore, we switch to new coordinates $\tilde{q}_\alpha = [\tilde{\alpha}_l, \tilde{\alpha}_t]^{\mathsf{T}}$, defined as

$$\tilde{q}_\alpha = \tilde{S} q_\alpha + c_\alpha, \quad (23)$$

where $\tilde{S} = [1, 0; 1, 1]$ and vector c_α is chosen to cancel the constant term $G_{0\alpha}$. Let us write the mass matrix H_α and the potential term $G_{1\alpha}$ as

$$H_\alpha = \tilde{S}^\mathsf{T} \tilde{H}_\alpha \tilde{S}, \quad G_{1\alpha} = \tilde{S}^\mathsf{T} \tilde{G}_{1\alpha} \tilde{S}. \tag{24}$$

Then the equations of motion in $\alpha \in \{\phi, \theta\}$ sectors become

$$\tilde{H}_\alpha \ddot{\tilde{q}}_\alpha + \tilde{G}_{1\alpha} \tilde{q}_\alpha = 0, \tag{25}$$

where $\tilde{H}_\alpha$ and $\tilde{G}_{1\alpha}$ are

$$\tilde{H}_\alpha = \begin{bmatrix} \tilde{\mu}_2 + I_{1\alpha} & -m_2 l_h l_t \\ -m_2 l_h l_t & m_2 l_t^2 + I_{2\alpha} \end{bmatrix},$$
$$\tilde{G}_{1\alpha} = g \begin{bmatrix} -\tilde{\mu}_1 & 0 \\ 0 & m_2 l_t \end{bmatrix}, \tag{26}$$

and the term c_α was set to $(\tilde{S}^\mathsf{T} \tilde{G}_{1\alpha})^{-1} G_{0\alpha}$:

$$c_\alpha = \begin{bmatrix} -\delta_{\alpha\phi} \frac{\mu_0 d}{\tilde{\mu}_1} \\ 0 \end{bmatrix}. \tag{27}$$

Note that $\tilde{G}_{1\alpha}$ (and $G_{1\alpha}$) does not depend on α, but we keep the subscript to distinguish it from G_1.

Projecting the equations of motion onto phase II, (see Eq. (16)), we find that the ϕ sector reduces to ϕ_t governed by the equation

$$\left(m_2 l_t^2 + I_{2\phi}\right) \ddot{\phi}_t + g m_2 l_t \phi_t = 0, \tag{28}$$

while the θ sector equations remain unchanged, and the ψ sector is absent in phase II.

IV. SOLUTION SYMMETRIES AND CONSTRAINTS

Similarly to Ref. [11], we will impose certain symmetry constraints on the form of the solution of Eq. (15). This will reduce the number of equations we need to consider and will make the problem more manageable, which is especially important for an analytical investigation.

The model Lagrangian, and therefore the derived equations of motion, are invariant with respect to time reversal and a spatial reflection across a vertical plane. Therefore, a collisionless solution remains valid under these transformations. Due to the model's sagittal and coronal plane symmetries, we can look for a solution that is invariant to simultaneous time reversal and spatial reflections. Specifically, we require the invariance of the solution in phase I under $(t, x) \rightarrow -(t, x)$, and in phase II under $(t, x, y) \rightarrow -(t, x, y)$ [where (t, x, y) are measured relative to certain symmetry points]. We call these symmetry points P_s and P_d, for the single and double support phases, respectively. In terms of the generalized coordinates, the solution is invariant under the following transformations:

$$P_s : \quad (t, \theta_l, \psi_l, \theta_t) \rightarrow -(t, \theta_l, \psi_l, \theta_t),$$
$$P_d : \quad (t, \theta_l, \phi_l, \theta_t) \rightarrow -(t, \theta_l, \phi_l, \theta_t). \tag{29}$$

The generalized coordinates and their time derivatives are continuous functions of time at the symmetry points. Therefore, if a coordinate flips sign in Eqs. (29), the coordinate and its even order time derivatives must vanish at the symmetry point. Otherwise, the odd order time derivatives vanish. Notice also that the symmetry of P_d implies that the walker is in the upright configuration at P_d.

Thanks to the symmetries of Eqs. (29), the complete walking cycle can be obtained from the part of the trajectory connecting nearby points P_s and P_d that makes up a quarter of the cycle. Thus, it is sufficient to focus on the solution between the two symmetry points.

The transition from phase I to phase II is punctuated by a foot impact event. In a time-reversed picture, in the phase II to phase I transition, this event would normally be viewed as a foot liftoff. We will refer to it as an impact in either case.

Let $q^s(t)$ be the result of integrating the equations of motion $D^s q^s = 0$ forward in time starting from P_s. Let $q^d(t)$ be the result of integrating the equations of motion $D^d q^d = 0$ backward in time starting from P_d. Let t_s and $-t_d$ be the moment of time t where the respective branches reach the impact point. For a collisionless impact, it is required [8] that the swing foot position r [of the branch $q^s(t)$] satisfies at the impact $\dot{r} = \ddot{r} = 0$. Since the foot positions are not affected by θ_l rotations, and $\phi_l = 0$ in phase II, the impact conditions translate into $\phi_l^s = \dot{\phi}_l^s = \dot{\psi}_l^s = \ddot{\phi}_l^s = \ddot{\psi}_l^s = 0$ at $t = t_s$. We can write the impact conditions as

$$D^i q^s(t_s) = 0, \tag{30}$$

where $D^i_{(1,1)} = 1$, $D^i_{(2,1)} = D^i_{(3,3)} = \frac{d}{dt}$, $D^i_{(4,1)} = D^i_{(5,3)} = \frac{d^2}{dt^2}$, and the rest are zeros. For $q^s(t)$ and $q^d(-t)$ to belong to the same solution, the model states from two branches must match at the impact: $J^d q^s(t_s) = q^d(-t_d)$ and $J^d \dot{q}^s(t_s) = \dot{q}^d(-t_d)$. We can write the matching conditions as

$$D^m(J^d q^s(t_s) - q^d(-t_d)) = 0, \tag{31}$$

where $D^m = [I; I\frac{d}{dt}]$.

To find a valid collisionless solution, there are 11 constraints to be satisfied: five from Eq. (30) and six from Eq. (31). We will refer to them as joining conditions, as they are imposed at the joining point of two branches. If the model is fixed, the number of free parameters that can be varied is 10: eight initial conditions on the parameters that are invariant to the symmetry transformations Eqs. (29), namely, $(\phi_l, \dot{\theta}_l, \psi_l, \phi_t, \dot{\theta}_t)|_{t=0}$ for P_s and $(\dot{\theta}_l, \dot{\phi}_t, \dot{\theta}_t)|_{t=0}$ for P_d, and two impact times, t^s and t^d. Even if all the parameters are independent (which is not the case in the linear dynamics limit, as we show later), it is not possible to construct a lossless gait without tuning the model parameters.

We can generalize this consideration to other models with periodic collisionless solutions [8,9,11]. In general, let P_s and P_d be the symmetry points in the less constrained (phase I) and more constrained (phase II) phases, respectively. In a symmetry point, for every degree of freedom, either its coordinate or velocity turns zero. A collisionless solution is invariant with respect to a sign flip in time and in every component turning zero. Let $n_s = \dim(q^s)$ and $n_d = \dim(q^d)$. We define the impact dimension d_i as the number of degrees that freeze (become inactive, in other words) upon transitioning from phase I to phase II: $d_i = n_s - n_d$. Let n_e be the number of parameters encoding the impact surface. In general, $n_e = \dim(\text{space}) - \dim(\text{ground})$, so $n_e = 1$ in all the cited cases. The number of adjustable solution parameters is $n_s + n_d + 2$: one from each degree of freedom (nonzero coordinate or velocity) plus the impact time, for both phases. The number of joining conditions is $n_e + 2d_i + 2n_d$: $n_e + 2d_i$ impact conditions and $2n_d$

matching conditions. Thus, the number of model parameters requiring tuning is $n = (n_e + 2d_i + 2n_d) - (n_s + n_d + 2) = d_i + n_e - 2$. Note that in general n_e can differ from 1; for example, $n_e = 2$ for a three-dimensional tightrope walker.

V. SMALL MOVEMENT LIMIT SOLUTION

In the SML, the equations in the ϕ and θ sectors are linear. While the equation on ψ is nonlinear, it can be easily integrated analytically. However, the need to coordinate motion in three planes to satisfy the joining conditions of a collisionless solution leads to nontrivial nonlinear equations on the impact times and normal mode frequencies. These equations are difficult to analyze in their generality. In this section, the analysis is simplified by imposition of an additional constraint and a formulation in terms of dimensionless impact phases. Also, we will focus our attention on the least exotic walking solution, that is, a solution with the fewest oscillations.

A. Axial plane solution

To distinguish quantities in phases I and II, we optionally use the phase notation $p \in \{s, d\}$ that assumes the value s in phase I (single support) and the value d in phase II (double support). To reduce clutter we omit the sector ψ and phase s superscripts in this section, listing all the affected quantities at the end.

Integrating Eq. (20), we find

$$\psi_l(t) = wt - I_\psi^{-1}\Bigg(db^{\mathsf{T}} q_\theta(t) + \int_0^t dt'\big(q_\phi^{\mathsf{T}}(t')A_{\phi\theta}\dot{q}_\theta(t') + q_\theta^{\mathsf{T}}(t')A_{\theta\phi}\dot{q}_\phi(t')\big)\Bigg). \tag{32}$$

Note, a constant term in the above expression is absent due to the symmetry of P_s [see Eqs. (29)], dictating that $\psi_l(t)$ and $q_\theta(t)$ be odd functions, and $q_\phi(t)$ to be an even function.

To significantly simplify our analysis of the SML solution, we will impose an additional constraint on it, requiring the vanishing of q_θ at the impact:

$$q_\theta(t_s) = 0. \tag{33}$$

We call it the upright legs at impact (ULI) constraint, as it implies the same configuration of the legs, as in the upright configuration. As will be explained in Sec. V C, in the SML, $q_\theta(t)$ realizes a simple harmonic motion and, therefore, the ULI constraint also implies $\ddot{q}_\theta(t_s) = 0$. To satisfy the constraint, we will need to tune an additional model parameter. The constraint is imposed only in the SML and not on the general solution.

There are two joining equations involving $\psi_l(t)$:

$$\begin{aligned} \dot{\psi}_l(t_s) &= 0, \\ \ddot{\psi}_l(t_s) &= 0. \end{aligned} \tag{34}$$

Both equations arise from the impact conditions Eq. (30). Under the ULI constraint, the joining conditions in Eqs. (34) translate respectively to

$$\begin{aligned} w - I_\psi^{-1}\big(db^{\mathsf{T}} + q_\phi^{\mathsf{T}}(t_s)A_{\phi\theta}\big)\dot{q}_\theta(t_s) &= 0, \\ \dot{q}_\phi^{\mathsf{T}}(t_s)\big(A_{\phi\theta} + A_{\theta\phi}^{\mathsf{T}}\big)\dot{q}_\theta(t_s) &= 0. \end{aligned} \tag{35}$$

At the impact point, $\dot{\phi}_l(t_s) = 0$, see Eq. (30). This also implies $\dot{\phi}_t(t_s) \neq 0$, because otherwise $[q_\phi(t_s); \dot{q}_\phi(t_s)]$ would be a singular point on the phase portrait of the ϕ sector dynamics (which is decoupled from other sectors in the SML), which would be incompatible with a periodic walking solution we are looking for. Therefore, the second joining condition becomes

$$b_1^{\mathsf{T}} \dot{q}_\theta(t_s) = 0, \tag{36}$$

where $b_1 = (\tilde{S}^{-1})^{\mathsf{T}}(A_{\phi\theta}^{\mathsf{T}} + A_{\theta\phi})_{(\cdot 2)} = [-I_{2\phi}; I_{2\theta} - I_{2\psi}]$.

In this section, we have omitted ψ and s superscripts in ψ_l^s, $w^{\psi s}$, q_θ^s, q_ϕ^s, ϕ_l^s, and ϕ_t^s.

B. General form of linear dynamics solution in sagittal and coronal sectors

Let us investigate Eq. (25), which describes motion in both the coronal ($\alpha = \phi$) plane in phase I, and sagittal ($\alpha = \theta$) plane in phases I and II. To reduce notational clutter, we will be omitting the sector α and phase p sub- and superscripts throughout this section. To eliminate ambiguity, we provide a list of affected quantities in full notation at the end of the section. Let us introduce a matrix M,

$$M = -\tilde{G}_1^{-1}\tilde{H} = \begin{bmatrix} a_+ & -\gamma\beta^{-1} \\ \gamma\beta & a_- \end{bmatrix}, \tag{37}$$

where

$$\begin{aligned} a_+ &= \frac{\tilde{\mu}_2 + I_1}{g\tilde{\mu}_1}, \quad a_- = -\frac{m_2 l_t^2 + I_2}{g m_2 l_t}, \\ \beta &= \sqrt{\frac{\tilde{\mu}_1}{m_2 l_t}}, \quad \gamma = \frac{l_h}{g\beta}. \end{aligned} \tag{38}$$

Let $\{\lambda_z, u_z\}|_{z=\pm}$ be the eigensystem of M. The subscript z represents ± 1, which we often shorten to $\pm$. Notice that $\det M < 0$, because $\tilde{H}$ is positive definite and $\det \tilde{G}_1 < 0$, see Eqs. (26). Therefore, M has two real eigenvalues, one positive and one negative (see Appendix I for details): $\lambda_+ > 0$ and $\lambda_- < 0$. The general solution of Eq. (25) can be written as

$$\tilde{q}(t) = \sum_{zz'=\pm 1} w_{zz'} u_z e^{\frac{z't}{\sqrt{\lambda_z}}}, \tag{39}$$

where $w_{zz'}$ are the weights of different normal modes. Let us define a function

$$\Lambda_{zz'}(a, b, c) = \tfrac{1}{2}\big(a + zb + z'\sqrt{(a-b)^2 + 4c}\big) \tag{40}$$

and shorthand notations

$$\begin{aligned} \lambda_{zz'} &\equiv \Lambda_{zz'}(a_+, a_-, -\gamma^2), \\ a_{zz'} &\equiv \Lambda_{zz'}(\lambda_+, \lambda_-, \gamma^2). \end{aligned} \tag{41}$$

We can now compactly write down the eigensystem of M,

$$\lambda_z = \lambda_{+,z}, \quad u_z = [\lambda_{-,z}, \gamma\beta]^{\mathsf{T}}, \tag{42}$$

and the expression of a_z in terms of λ_z and γ:

$$a_z = a_{+,z}. \tag{43}$$

The general solution of the phase II Eq. (28) is

$$\phi_t(t) = \sum_{z=\pm 1} w_z e^{\frac{zt}{\sqrt{a_-}}}.$$ (44)

The quantities in this section that have the sector α and phase p sub- or superscript in their full notations include M_α, $\tilde{G}_{1\alpha}$, $\tilde{H}_\alpha$, a_z^α, $I_{i\alpha}$, $\lambda_z^{\alpha p}$, $u_z^{\alpha p}$, $\tilde{q}_\alpha^p$, $w_{zz'}^{\alpha p}$, $\lambda_{zz'}^{\alpha p}$, and $a_{zz'}^{\alpha p}$.

We will be using a frequency notation $\omega_z^{\alpha p} \equiv 1/\sqrt{z\lambda_z^{\alpha p}}$ in the following analysis. If a quantity does not depend on the phase index p, as is the case for $\lambda_z^{\theta p}$, $u_z^{\theta p}$ and $\omega_z^{\theta p}$, we will omit p for clarity.

C. Sagittal plane solution

To reduce clutter, we omit the sector θ superscript in this section, listing the affected quantities at the end.

According to Eqs. (29), the symmetries of P_s and P_d dictate that $\tilde{q}_\theta^p(t)$ be an odd function in both phases. Therefore, the weights $w_{zz'}^p$ in Eq. (39) must be odd functions of z'. Consequently, the sagittal plane solution must be in the form

$$\tilde{q}_\theta^p(t) = w_+^p u_+ \sinh \omega_+ t + w_-^p u_- \sin \omega_- t,$$ (45)

where we have defined $w_z^p = 2z\sqrt{z}z'w_{zz'}^p$. There are four scalar joining equations involving the sagittal sector:

$$\tilde{q}_\theta^s(t_s) - \tilde{q}_\theta^d(-t_d) = 0,$$
$$\dot{\tilde{q}}_\theta^s(t_s) - \dot{\tilde{q}}_\theta^d(-t_d) = 0.$$ (46)

All the equations arise from the matching conditions Eq. (31). Because the equations of motion are identical in both phases, a formal continuation of either branch $\tilde{q}_\theta^p(t)$ to all t is a valid solution (up to a time shift), and

$$\tilde{q}_\theta^s(t) = \tilde{q}_\theta^d(t - t_s - t_d).$$ (47)

Since the solution is periodic and the first term in the right hand side of Eq. (45) is unbounded, its weight must be $w_+ = 0$ and the sagittal sector motion in both phases is a simple harmonic motion $\tilde{q}_\theta^p(t) \propto \sin \omega_- t$. It then follows from Eq. (47):

$$\omega_-(t_s + t_d) = \pi k, \ k \in \mathbb{Z}$$ (48)

(where $\mathbb{Z}$ is the set of integer numbers) and $w_-^s = (-1)^k w_-^d$. The ULI constraint of Eq.(33) implies $\omega_- t_s = \pi k'$, $k' \in \mathbb{Z}$, and therefore $\omega_- t_d = \pi(k - k')$. In the rest of the analysis, we choose to consider a solution with the smallest positive t_p, therefore we pick $k = 2, k' = 1$ to have:

$$t_s = t_d = \frac{\pi}{\omega_-}.$$ (49)

Because we are focusing on a solution with $t_s = t_d$, we may use a single notation $\tau = t_s = t_d$ to represent the impact times in both phases. We introduce an impact phase notation $o_- = \omega_-\tau$, so the previous equation can be written as

$$o_- = \pi.$$ (50)

An impact phase describes the phase gained by a normal mode between $t = 0$ and the impact moment. The full utility of the impact phase notations will become evident in the next section.

In this section, we have omitted θ superscripts in: $w_{zz'}^{\theta p}$, $w_z^{\theta p}$, u_z^θ, ω_z^θ, and o_-^θ.

D. Coronal plane solution

To reduce notational clutter we omit the sector ϕ superscript in this section, listing all the affected quantities at the end.

According to Eqs. (29), the symmetries of P_s and P_d dictate that $\tilde{q}_\phi^s(t)$ and $\phi_t^d(t)$ be an even and odd functions respectively. Therefore, the weights $w_{zz'}^s$ in Eq. (39) must be an even function of z', while the weights w_z^d in Eq. (44) must be an odd function of z. Consequently, the coronal plane solution must have the form

$$\tilde{q}_\phi^s(t) = w_+^s u_+^s \cosh \omega_+^s t + w_-^s u_-^s \cos \omega_-^s t,$$
$$\phi_t^d(t) = w^d \sin \omega^d t,$$ (51)

where we have defined $w_z^s = 2w_{zz'}^s$, $w^d = -2izw_z^d$ and $\omega^d = 1/\sqrt{-a_-}$. There are five joining equations involving the coronal sector:

$$\tilde{\phi}_l^s(t_s) - c_{\phi(1)} = 0,$$
$$\dot{\tilde{\phi}}_l^s(t_s) = 0,$$
$$\ddot{\tilde{\phi}}_l^s(t_s) = 0,$$
$$\tilde{\phi}_t^s(t_s) - \phi_t^d(-t_d) = 0,$$
$$\dot{\tilde{\phi}}_t^s(t_s) - \dot{\phi}_t^d(-t_d) = 0.$$ (52)

The first three equations arise from the impact conditions Eq. (30), while two other equations arise from the matching conditions Eq. (31) (the last two equations were simplified using the first two). The five joining conditions form a set of linear equations on $w = [w_+^s, w_-^s, w^d]^\mathsf{T}$. The first equation determines the scale of the solution of the homogeneous linear system $A(t_s, t_d)w = 0$, comprised of the other four equations. The matrix $A(t_s, t_d)$ is a 4×3 matrix, whose coefficients are functions of t_s and t_d. For a nontrivial w solution to exist, the rank of A must be lowered below 3. This can be achieved by appropriately tuning t_s and t_d. To that end, we have derived the following equations on t_p, (see Appendix E for details):

$$\omega_-^s \cot \omega_-^s t_s = \omega_+^s \coth \omega_+^s t_s,$$
$$\omega_-^s \cot \omega_-^s t_s = \omega^d \tan \omega^d t_d.$$ (53)

Because the equation of motion in phase II is a projection of the phase-I equations, the frequencies ω_z^s and ω^d are not independent, they satisfy (see Appendix I)

$$(a_- - \lambda_-)(a_- - \lambda_+) = \gamma^2.$$ (54)

As discussed in the previous section, we consider a solution with $t_s = t_d = \tau$. We can view Eqs. (53) and (54) as a system of equations on the ϕ sector spectrum, given the impact time τ. We can write them as

$$o_+ \coth o_+ = o_- \cot o_- = o \tan o,$$
$$(o^{-2} - o_-^{-2})(o^{-2} + o_+^{-2}) = \bar{\tau}^{-4},$$ (55)

where we have introduced the impact phase notations $o_z = \omega_z^s \tau$, $o = \omega^d \tau$ and the reduced impact time notation $\bar{\tau} = \tau/\sqrt{\gamma}$. Interestingly, the equations in Eqs. (55) are free of any model parameters. In that sense, the impact phases are universal. We refer to them, and any other functions derived
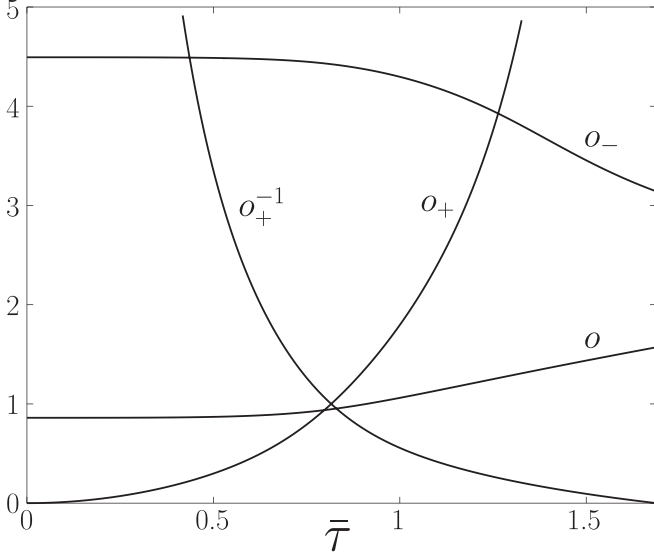
FIG. 2. The impact phases $o_+(\bar{\tau})$, $o_-(\bar{\tau})$, and $o(\bar{\tau})$ are functions of the reduced impact time $\bar{\tau} \in (0, \bar{\tau}_c)$. Because o_+ is unbounded, it is plotted together with $1/o_+$.

from the impact phases and the reduced impact time alone, as universal functions.

Since τ and the frequencies are positive, we are only concerned with positive roots of Eqs. (55). Since $o_+ \coth o_+ \geqslant 1$, both o_- and o can only belong to $(k\pi, (k + 1/2)\pi)$, $k \in \mathbb{Z}$, where $\tan()$ is positive. Since $o_- \cot o_- \leqslant 1$ for $o_- < \pi/2$, we need $k > 0$ for o_-. The parameter k characterizes how many oscillating movements the walker commits before the impact. We choose to look for a solution with the minimal number of such oscillations, therefore we limit our consideration to $o_- \in (\pi, 3\pi/2)$ and $o \in (0, \pi/2)$ in the rest of this section. Under these constraints, $o_+ \coth o_+$, $o_- \cot o_-$, and $o \tan o$ are monotonic functions of their arguments. It then follows from the first line of Eqs. (55) that o_+ and o are monotonically decreasing functions of o_-. From the second line of Eqs. (55), it follows that $\bar{\tau}$ is also a monotonically decreasing function of o_-. Therefore, all the impact phases are monotonic functions of $\bar{\tau}$: o_- is decreasing, while o_+ and o are increasing functions. The solution of Eqs. (55), $o_+(\bar{\tau})$, $o_-(\bar{\tau})$, and $o(\bar{\tau})$ are plotted in Fig. 2. It is straightforward to find

$$
\begin{aligned}
o_+(\bar{\tau}) &\in (0, +\infty), \\
o_-(\bar{\tau}) &\in (\pi, o_{-u}), \\
o(\bar{\tau}) &\in \left(o_l, \frac{\pi}{2}\right), \\
\bar{\tau} &\in (0, \bar{\tau}_c),
\end{aligned}
\tag{56}
$$

where $o_{-u} = 4.4934094\ldots$ and $o_l = 0.86033359\ldots$ are the roots of $o_- \cot o_- = 1$ and $o \tan o = 1$, respectively, and $\bar{\tau}_c = \pi/\sqrt{2\sqrt{3}}$. It is straightforward to extract the asymptotic behavior of impact phases for the extreme values of $\bar{\tau}$. For $\bar{\tau} \to 0$, to two dominant terms, we find

$$
o_z \to v_z^0 \bar{\tau}^{z+1}\left(1 + z v_z^1 \bar{\tau}^4\right), \quad o \to v_0(1 + v_1 \bar{\tau}^4),
\tag{57}
$$

where

$$
\begin{aligned}
v_+^0 &= \sqrt{o_l^{-2} - o_{-u}^{-2}}, \quad v_-^0 = o_{-u}, \quad v_0 = o_l, \\
v_+^1 &= \frac{1}{2}\left(o_l^{-2} - o_{-u}^{-2}\right)o_l^{-2} - \frac{1}{3}\left(\left(o_l^2 + 2\right)^{-1}o_l^{-2} - o_{-u}^{-3}\right), \\
v_-^1 &= \frac{1}{3}\left(o_l^{-2} - o_{-u}^{-2}\right)o_{-u}^{-1}, \\
v_1 &= \frac{1}{3}\left(o_l^{-2} - o_{-u}^{-2}\right)\left(o_l^2 + 2\right)^{-1}.
\end{aligned}
\tag{58}
$$

For $\bar{\tau} \to \bar{\tau}_c$, to the lowest nonconstant term, we find

$$
\begin{aligned}
o_+ &\to \frac{4}{3}\epsilon^{-1}, \quad o_- \to \pi\left(1 + \frac{3}{4}\epsilon\right), \\
o &\to \frac{\pi}{2}\left(1 - \frac{3}{4}\epsilon\right),
\end{aligned}
\tag{59}
$$

where $\epsilon = -(\bar{\tau} - \bar{\tau}_c)/\bar{\tau}_c$.

In this section, we have omitted ϕ superscripts in $w_{zz'}^{\phi s}$, $w_z^{\phi p}$, $w^{\phi d}$, $u_z^{\phi s}$, $\omega_z^{\phi s}$, $\omega^{\phi d}$, a_-^ϕ, λ_z^ϕ, o_z^ϕ, o^ϕ, o_{-u}^ϕ, and o_l^ϕ.

E. Model parametrization of the collisionless solution

So far, we have resolved the joining conditions in the coronal and sagittal sectors in terms of the impact phases o_z^ϕ, o^ϕ, and o_-^θ. In the axial sector, out of two joining conditions one [the first in Eqs. (35)] can always be trivially satisfied, while the other [Eq. (36)] remains to be solved. To complete the SML solution, we need to select physically admissible values of the model parameters that reproduce the impact phases and solve the remaining joining condition, Eq. (36). That can be done, in fact, for any $\bar{\tau} \in (0, \bar{\tau}_c)$, as we show in this section.

The physically realizable model parameter values must satisfy the following constraints: The parameters l_i, l_h, l_t, m_i, and $I_{i\alpha}$, where $i \in \{1, 2\}$ and $\alpha \in \{\phi, \theta, \psi\}$, must all be non-negative. In addition, the moments of inertia must respect the triangle inequality: $I_{i\alpha_1} + I_{i\alpha_2} \geqslant I_{i\alpha_3}$, for all distinct α_i.

In Sec. IV, we provided a counting argument showing that at least one model parameter needs to be tuned to obtain a collisionless solution. In the linear dynamics limit, the sagittal sector solution is defined up to an arbitrary scale ε. Setting this scale consumes an additional free parameter. Satisfying the ULI constraint takes another free parameter. Solving for an arbitrary $\bar{\tau}$ value consumes yet another free parameter. In total, we now need to adjust at least four model parameters.

We consider two parametrization prescriptions: a simpler (restricted) case and a more general case. We start by considering the restricted case, where we set to zero as many moments of inertia as possible to simplify consideration: $I_{1\phi} = I_{2\phi} = I_{1\theta} = 0$. The restricted case solution is then generalized to the general case of positive moments of inertia. While both cases are not totally general, they offer useful analytical insights about the extent of the domain of admissible model parameters. Refer to Appendix F for more details.

1. Restricted case parametrization

First, we find l_h, l_1, and τ, given a solution of the ϕ sector equations Eqs. (55). For compactness, we present the results

in dimensionless units by setting $g = m_2 = l_t = 1$,

$$l_h = \kappa_2(\kappa_1\sqrt{m_1} + 1), \quad l_1 = l_h\frac{\kappa_1}{\sqrt{m_1}}, \quad (60)$$

where the universal functions $\kappa_i(\bar{\tau})$ are completely independent of the model parametrization,

$$\kappa_1 = \sqrt{-\bar{\lambda}_+^\phi \bar{\lambda}_-^\phi}, \quad \kappa_2 = (\bar{a}_{+-}^\phi)^{-2}, \quad (61)$$

where $\bar{\lambda}_z^\phi = \lambda_z^\phi/\gamma = z(o_z^\phi(\bar{\tau})/\bar{\tau})^{-2}$ and $\bar{a}_{zz'}^\phi = a_{zz'}^\phi/\gamma = \Lambda_{zz'}(\bar{\lambda}_+^\phi, \bar{\lambda}_-^\phi, 1)$. For any $\bar{\tau} \in (0, \bar{\tau}_c)$, the functions κ_1 and κ_2 are positive and so are l_h and l_1. The condition $l_2 > 0$ is satisfied as long as $m_1 > m_c$, where

$$m_c = \begin{cases} 0, & \kappa_2 \geqslant 1 \\ \left(\frac{1-\kappa_2}{\kappa_1\kappa_2}\right)^2, & \kappa_2 < 1. \end{cases} \quad (62)$$

The impact time is

$$\tau = \bar{\tau}\kappa_2^{\frac{1}{4}}. \quad (63)$$

Next, we need to find $I_{2\theta}$. Notice its value does not affect ϕ sector. Equation (50) (which is a consequence of the ULI constraint) can be solved for a positive $I_{2\theta}$ given any $\bar{\tau} \in (0, \bar{\tau}_c)$. Indeed, if $I_{2\theta} = 0$, then $o_-^\theta = o_-^\phi > \pi$, and if $I_{2\theta} \to +\infty$, then $o_-^\theta \to 0$. Therefore, there exists $I_{2\theta} > 0$ that solves $o_-^\theta = \pi$:

$$I_{2\theta} = \frac{\tau^2}{\pi^2} + \left(\frac{\tau^2}{\pi^2}\kappa_2^{-1} + \kappa_1^2 + 1\right)^{-1} - 1. \quad (64)$$

To respect the triangle inequalities on the moments of inertia, one should set $I_{1\psi} = 0$ and $I_{2\psi} = I_{2\theta}$. Coincidentally, this choice of I_2 parameters also satisfies the axial plane joining condition Eq. (36), as $b_1 = 0$ now. Thus, the restricted case SML solution is parametrized by four independent parameters: two model parameters (d and m_1), and two nonmodel parameters ($\bar{\tau}$ and ε).

To restore the presented expressions to dimensionful notations, one needs to replace all mass m_a, length l_a, moment of inertia I_a, and time τ notations with m_a/m_2, l_a/l_t, $I_a/m_2l_t^2$, and $\tau\sqrt{g/l_t}$, respectively, where a stands for any subscript.

2. General case parametrization

To consider the general case of positive moments of inertia, we parametrize them as $I_{1\alpha} = c_1^\alpha\tilde{\mu}_2$ and $I_{2\alpha} = c_2^\alpha m_2l_t^2$. While $I_{1\alpha}$ is now parametrized implicitly (since $\tilde{\mu}_2$ is not fixed), this type of analysis still gives us a good idea about the range of $I_{1\alpha}$ values, for which an admissible parametrization of the SML solution exists. Let us define

$$\kappa_1' = \sqrt{\frac{\kappa_1^2 + 1}{(1 + c_1^\phi)(1 + c_2^\phi)} - 1}, \quad (65)$$
$$\kappa_2' = \kappa_2(1 + c_2^\phi)^2.$$

If we now replace κ_i with κ_i' in Eqs. (60), (62), and (63), we obtain the general case solution for l_h, l_1 m_c, and τ, (see Appendix F for more details). The solution is defined for those values of $\bar{\tau}$ and c_i^ϕ that do not turn the expression under the square root in Eqs. (65) negative. The general case formula

for $I_{2\theta}$ involves more than just replacing κ_i with κ_i':

$$I_{2\theta} = \frac{\tau^2}{\pi^2} + \left(\frac{\tau^2}{\pi^2}\kappa_2'^{-1} + \left(\kappa_1'^2 + 1\right)\left(1 + c_1^\theta\right)\right)^{-1} - 1. \quad (66)$$

Let us investigate the case of $I_{2\phi} = I_{2\theta} = \zeta$. In this case, ζ dependence drops out of Eq. (66) completely, and we can rewrite it as

$$c_1^\theta = \left(1 + c_1^\phi\right)\frac{(1 - \xi^2)^{-1} - \xi^2\kappa_2^{-1}}{\kappa_1^2 + 1} - 1, \quad (67)$$

where $\xi = \bar{\tau}\kappa_2^{1/4}/\pi$. The equation has the form $c_1^\theta = (1 + c_1^\phi)\Phi(\xi, \kappa_1, \kappa_2) - 1$; it is easy to verify (see Appendix F for details) that $\Phi(\xi, \kappa_1, \kappa_2) > 1$ as long as $\xi < 1$, and therefore, $c_1^\theta > c_1^\phi$. Thus, we have an explicit prescription, in terms of c_i^α, for the model parametrization in the general case for any $\bar{\tau}$, as long as $(1 + c_1^\phi)(1 + \zeta) < \kappa_1^2 + 1$.

To have a more quantitative assessment of the admissible model parameter domain, we present the asymptotic expansion of κ_i to the lowest nonconstant term, as well as the expansion of $\bar{\lambda}_z$ to the lowest order needed to establish the expansion of κ_i. For $\bar{\tau} \to 0$, we find from Eqs. (57), (58), and (61):

$$\bar{\lambda}_z \to z\nu_z^{0-2}\bar{\tau}^{-2z}\left(1 - 2z\nu_z^1\bar{\tau}^4\right) \quad (68)$$

and

$$\begin{aligned}\kappa_1 &\to (\nu_+^0\nu_-^0)^{-1}(1 - (\nu_+^1 - \nu_-^1)\bar{\tau}^4), \\ \kappa_2 &\to \nu_0^4\bar{\tau}^{-4}.\end{aligned} \quad (69)$$

For $\bar{\tau} \to \bar{\tau}_c$, we find from Eqs. (59) and (61):

$$\bar{\lambda}_+ \to \frac{3\sqrt{3}}{32}\pi^2\epsilon^2, \quad \bar{\lambda}_- \to -\frac{1}{2\sqrt{3}}\left(1 - \frac{7}{2}\epsilon\right) \quad (70)$$

and

$$\kappa_1 \to \frac{\sqrt{3}}{8}\pi\epsilon, \quad \kappa_2 \to \frac{3}{4}(1 + \epsilon). \quad (71)$$

The functions κ_i and ξ are plotted in Fig. 3. We have verified that κ_i are monotonically decreasing functions, while ξ is a monotonically increasing function of $\bar{\tau}$. The function ξ changes from $\xi \to \nu_0/\pi$ at $\bar{\tau} \to 0$ to $\xi \to 1/2$ at $\bar{\tau} \to \bar{\tau}_c$. Thus, the required condition $\xi < 1$ is satisfied for all $\bar{\tau}$. Notice that $\tau \to \nu_0\sqrt{1 + c_2^\phi}$ remains finite for $\bar{\tau} \to 0$.

The axial joining condition Eq. (36) is equivalent to $b_1^\mathsf{T}u_-^\theta = 0$, from where we find, for $I_{2\phi} = I_{2\theta} = \zeta$: $I_{2\psi} = \zeta(1 - u_{-(1)}^\theta/u_{-(2)}^\theta)$. Since $0 < u_{-(1)}^\theta < u_{-(2)}^\theta$, (see Appendix F for details), we have $0 < I_{2\psi} < \zeta$, which satisfies the triangle inequality. To satisfy it for I_1, we choose $I_{1\psi}$ in the range $|I_{1\phi} - I_{1\theta}| \leqslant I_{1\psi} \leqslant I_{1\phi} + I_{1\theta}$. Thus, the general case SML solution is parametrized by seven independent parameters: five model parameters (d, m_1, c_1^ϕ, c_2^ϕ, and $I_{1\psi}$), and two nonmodel parameters ($\bar{\tau}$ and ε).

We have demonstrated that both the restricted and general case of the model parametrization satisfies all the joining equations and the ULI constraint, and therefore realizes a collisionless solution in the SML.

It is instructional to evaluate the effective number of the tuned model parameters in the restricted and general cases.
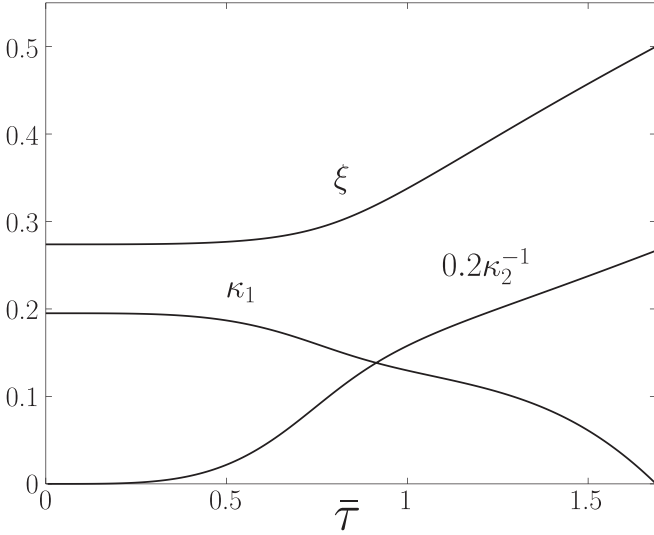
FIG. 3. Universal functions $\kappa_i(\bar{\tau})$ and $\xi(\bar{\tau})$ [plotted for $\bar{\tau} \in (0, \bar{\tau}_c)$] are independent of the model parametrization. Because κ_2 is unbounded from above, it is plotted as $0.2/\kappa_2$.

We ignore the nonholonomic constraints, even when they become degenerate, as in the restricted case. We also ignore the general case constraint $c_2^\phi = c_2^\theta$, which can be replaced by a nonholonomic constraint. Then, in both the restricted and general case, we only need to tune two additional model parameters to satisfy the ULI constraint and the axial joining condition. It makes four parameters in total (together with l_h and l_1), as expected.

F. Spring-supported torso solution

In this section, we consider a version of the original model endowed with torsion springs at the hip joint. This modification enables consideration of a collisionless gait with the torso located above the hip joint, which can be regarded as a more anthropomorphic-looking gait.

The hip springs are modeled by adding the elastic energy term

$$V_e = \frac{\text{k}}{2} q_t^\mathsf{T} q_t \tag{72}$$

to the potential energy V, where k is the spring constant. This changes the potential term G by ∇V_e in the equations of motion Eq. (15), without affecting H and C. In the SML, only G_1 is affected and only in $\alpha \in \{\phi, \theta\}$ sectors, cf. Eqs. (18) and (19):

$$G_{1\alpha} = g \begin{bmatrix} -\mu_1 & m_2 l_t \\ m_2 l_t & m_2 l_t + \frac{\text{k}}{g} \end{bmatrix}. \tag{73}$$

Note the same equations can be used for describing both the hanging and standing torso arrangements by choosing $l_t < 0$ for the standing torso case. As long as the choice of model parameters does not affect the signs of the eigenvalues of M in Eq. (37), all the analysis in terms of the impact phases in Sec. V C and V D, as well as the universal functions, remain unchanged. Only the model parametrization step needs to be reconsidered. Rather than reproducing a somewhat tedious analysis of Sec. V E for an arbitrary k of the spring-endowed

model, we take a different and simpler route. We establish an up-down torso duality, that connects solutions at different k values and l_t signs. We then use this duality to resolve the parametrization of the spring-supported standing torso solution in terms of the already solved springless hanging-torso solution parametrization.

We switch to dimensionless units $g = m_2 = 1$, $l_t = z = \pm 1$ with $z = -1$ corresponding to the standing torso setup. We generalize $\tilde{S}$ so it covers both values of z and matches $z = 1$, k = 0 case of Sec. III B,

$$\tilde{S} = \begin{bmatrix} 1 & 0 \\ \text{y} & z \end{bmatrix}, \tag{74}$$

where $\text{y} = 1/(z + \text{k})$ is chosen to make $\tilde{G}_{1\alpha}$ diagonal. We only use α for $\alpha \in \{\phi, \theta\}$ sectors. We use the prime to denote the quantities in the dual setup, corresponding to $z' = -z$. The duality relation is induced by requiring the parameters of the dual setup to be selected so $\tilde{H}_\alpha$ and $\tilde{G}_{1\alpha}$ are independent of z. Importantly, the joining conditions are independent of z in the α sectors (as one can easily verify). Therefore, provided the dual parameter values are physically admissible, the solution $\tilde{q}'_\alpha = \tilde{q}_\alpha$ is a valid collisionless solution, as it satisfies both the equations of motion and the joining conditions of the dual setup. In the ψ sector, the joining conditions do depend on z, requiring a proper selection of $I_{2\psi}$, as we explain at the end of this section.

We now present the explicit form of the duality transformation for all the model parameters, except $I_{2\psi}$. For simplicity, we keep $I_{i\alpha}$ fixed, only allowing k, m_1, l_1, and l_h to vary with z. Under these restrictions, we find for the duality transformation (see Appendix G for details)

$$\begin{aligned} z' &= -z, \\ \text{k}' &= \text{k} + 2z, \\ m'_1 &= \frac{\delta_1^2}{\delta_2}, \quad l'_1 = \frac{\delta_2}{\delta_1}, \\ l'_h &= l_h + 2z(1 + I_{2\alpha}), \end{aligned} \tag{75}$$

where we have defined

$$\begin{aligned} \delta_1 &= m_1 l_1 - 2z(2 + I_{2\alpha}), \\ \delta_2 &= m_1 l_1^2 - 4z(2 + I_{2\alpha})[l_h + z(1 + I_{2\alpha})]. \end{aligned} \tag{76}$$

For m'_1 and l'_1 to be physically admissible, the positivity of δ_i must be ensured, leading to the condition on m_1,

$$m_1 > (\max\{\sqrt{m_c}, \sqrt{m_{c1}}, \sqrt{m_{c2}}\})^2, \tag{77}$$

where

$$\sqrt{m_{c1}} = \left(\sqrt{1 + 8\frac{2 + I_{2\alpha}}{\kappa_2}} - 1 \right) \frac{1 + z}{4\kappa_1}, \tag{78}$$

$$\sqrt{m_{c2}} = 2\frac{2 + I_{2\alpha}}{\kappa_1^3 \kappa_2} \left(\sqrt{1 + \frac{1 + I_{2\alpha}}{2 + I_{2\alpha}}\kappa_1^2 + z} \right) - \frac{1}{\kappa_1}.$$

Note that μ_1, μ_2, and y do not change under the duality transformation.

Let us now consider the selection of $I_{2\psi}$, (which has no affect on the α sectors). In the restricted case, Eq. (36) is trivially satisfied (see Sec. V E 1), so $I'_{2\psi} = I_{2\psi}$. In the general

case, reproducing the analysis of Sec. V E 2 for general y and z, we find

$$I_{2\psi} = \zeta \frac{1 - xy}{1 + x(z - y)}, \qquad (79)$$

where $x = u_{-(1)}^{\theta}/u_{-(2)}^{\theta}$, $0 < x < \beta^{-1} < 1$ (see Appendix F) and $0 < y \leqslant 1$. To satisfy the triangle inequality on $I_{2\psi}$, we need $0 < I_{2\psi} < 2\zeta$, which is satisfied for any x if $z = 1$ and for $x < 1/(2 + y)$ if $z = -1$. From there a condition on m_1 follows (see Appendix G):

$$\sqrt{m_1} > \sqrt{m_{c3}} = \left(\frac{2 + y}{\sqrt{\kappa_2}} - 1 \right) \frac{1 - z}{2\kappa_1}. \qquad (80)$$

To obtain a standing torso solution parametrization in the general case, one can start with any valid springless model parametrization (as presented in Sec. V E), provided that the conditions Eqs. (77) and (80) are met. One then uses the duality transformation Eqs. (75) (with $z = 1$ and k = 0) and Eq. (79) (with $z = -1$ and y = 1) to compute all the model parameters in the dual setup. The restricted case is even simpler: only Eq. (77) needs to be enforced and instead of using Eq. (79) one sets $I_{2\psi}' = I_{2\psi}$.

Importantly, satisfying the conditions on m_1 poses no practical difficulty. It is straightforward to verify that, for a given springless solution, the conditions Eqs. (77) and (80) can always be satisfied by keeping $\bar{\tau}$ and $I_{i\phi}$ fixed, while increasing m_1 and computing all other parameters as prescribed by the springless model parametrization procedure. Note we do not need to know $\bar{\tau}'$, as the duality approach bypasses the use of the universal functions in the dual setup.

VI. GENERAL SOLUTION

Let χ include all the adjustable initial conditions on the generalized coordinates and the impact times, and let η include all the adjustable model parameters,

$$\begin{aligned} \chi &= \left[\phi_l^s, \phi_t^s, \dot{\theta}_l^s, \dot{\psi}_l^s, \dot{\theta}_t^s, \dot{\theta}_l^d, \dot{\phi}_t^d, \dot{\theta}_t^d, t_s, t_d \right]^{\mathsf{T}}, \\ \eta &= \left[l_h, l_1, d, m_1, \eta_I^{\mathsf{T}} \right]^{\mathsf{T}}, \end{aligned} \qquad (81)$$

where η_I is the triangle-inequality-respecting parametrization of the moments of inertia, see Appendix H for details. Thus, $x \equiv [\chi; \eta]$ includes all the parameters that can be adjusted while searching for a collisionless gait solution. Let $h(x)$ be 11-dimensional vector combining the joining conditions from Eqs. (30) and (31). We are interested in finding solutions of $h(x) = 0$, possibly with certain desired properties of x. A general solution can only be found numerically by an iterative procedure, such as Newton's method. In a complex high-dimensional problem without a good initial guess on x, this iterative procedure is not even guaranteed to converge to $h = 0$, let alone in a particular region with desired properties. Therefore, it is highly preferable that the initial guess x_0 be already close to the solution, that is, $h(x_0) \approx 0$. Our SML solution provides such x_0. We then evolve it to a desired region in the parameter space using a constrained gradient descent technique. It involves optimizing an objective function $f(x)$ of our choice, while staying close to a valid solution $h(x_i) \approx 0$ at any step i in the course of optimization. The constrained

gradient descent update rule is (see Appendix H for details)

$$x_{i+1} = x_i - \lambda_x^{-1} (I_x - h'(x_i)^+ h'(x_i)) \nabla f(x_i) - h'(x_i)^+ h(x_i), \qquad (82)$$

where the shorthand notation h' stands for the matrix $h'_{(ij)} \equiv \partial h_{(i)}/\partial x_{(j)}$, and h'^+ is a pseudoinverse of h' [defined for a matrix m as $m^+ = m^{\mathsf{T}}(mm^{\mathsf{T}})^{-1}$]. The second term on the right-hand side of the above equation is the projection of the gradient ∇f onto the tangent space of $h = 0$, while the last term enforces $h = 0$. The coefficient λ_x controls the gradient descent rate and $I_x \equiv I_{\dim(x) \times \dim(x)}$.

We use the general case parametrization for x_0, as prescribed in Sec. V E 2, with d set to a small value. We then evolve x away from the SML using Eq. (82) with f encoding certain soft constraints, for example, favoring larger values of d and penalizing excessively small values of l_h, l_1, and I_ϕ. We also penalize small values of $|\dot{\psi}_l(0)|$ to prevent collapse onto a purely coronal movement solution (side-to-side rocking with zero step length, i.e., $\psi_l = \theta_l = \theta_t = 0$). The optimization procedure was implemented using the freely available GNU OCTAVE software [18], and we found the optimization to be fairly straightforward.

Let the integers (k_ϕ, k_θ) be the numbers of oscillations in the coronal and sagittal sectors per one collisionless walking cycle. (Due to the imposed symmetries, the number of oscillations in the ϕ and θ sectors between two nearby symmetry points of the same type must be half-integer and integer, respectively, therefore k_ϕ and k_θ must be, respectively, odd and even.) We call such solution a (k_ϕ, k_θ) mode. So far, in Sec. V we have analyzed the (3,4) mode. As one stays near a valid solution during optimization, the discrete numbers (k_ϕ, k_θ) do not change, (perhaps with exception of certain points in the space of collisionless trajectories). To explore different general modes, one should seed the optimization with different SML modes. In the SML, it should be possible to analyze all the modes analytically, similarly to the (3,4) mode. This goes beyond the scope of the paper though, as the modes with a high number of oscillations seem less interesting for the purpose of walking. In the general regime, we focus exclusively on the (3,4) mode, which is the simplest SML mode compatible with the ULI constraint.

We have evolved the (3,4) mode from an initial general case SML solution (see Sec. V E 2) toward a nonsmall feet separation solution, following the outlined optimization procedure. We then truncated all but one of the model parameters to two significant digits and ran a few more iterations of the optimization step Eq. (82) with $\eta = [l_h]$ and $\nabla f = 0$, thus only optimizing over l_h to enforce $h = 0$. Our claim that a single model parameter suffices to tune a general collisionless mode is evidenced by a prompt drop of $\|h\|$ to the numerical zero. All the results presented below are for this particular solution, encoded by the following model parameter values: $l_h = 1.0941669$, $l_1 = 0.16$, $d = 0.15$, $m_1 = 0.19$, $I_{1\phi} = 0.00002$, $I_{1\theta} = I_{1\psi} = 0.00032$, $I_{2\phi} = 0.0000092$, $I_{2\theta} = I_{2\psi} = 0.019$ (we use $g = m_2 = l_t = 1$). The corresponding values of χ are given in Appendix I.

The torso's trajectory relative to the legs for the (3,4) mode is plotted in Fig. 4. The trajectory is loosely reminiscent of a Lissajous curve, as it is a closed contour of two superimposed
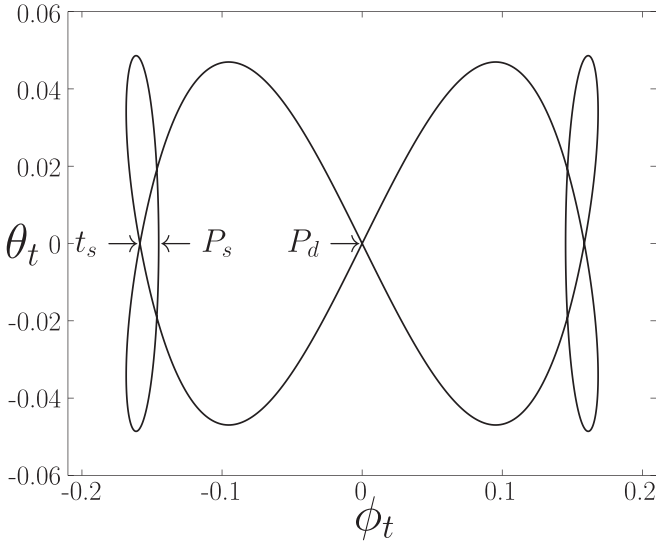
FIG. 4. The parametric plot of $\theta_t(t)$ vs $\phi_t(t)$ shows the torso's trajectory relative to the legs over one walking cycle for the (3,4) mode. The Lissajous-like curve features three coronal and four sagittal oscillations. The symmetry points P_s and P_d and the impact point (indicated here as t_s) are denoted in the left half of the plot.

FIG. 6. The first and second time derivatives (angular velocities and accelerations) that need to vanish at the impact for the solution to realize a collisionless conventional walking: $\dot{\phi}_l(t)$ (solid blue), $\dot{\psi}_l(t)$ (dash-dotted red), $\ddot{\phi}_l(t)$ (bold solid blue), and $\ddot{\psi}_l(t)$ (bold dash-dotted red) are plotted between P_s and impact. All the shown derivatives vanish at the impact.

oscillating motions, but only the sagittal oscillations are simple harmonic (and only in the SML).

A collisionless trajectory is fully specified by its definition between nearby symmetry points. In Fig. 5, we plot $q(t)$ between P_s and P_d, which constitutes a quarter of the cycle. A complete walking cycle trajectory can be obtained by unfolding the plot around the symmetry points with appropriate symmetry transformations. Note only ϕ_l vanishes at

the impact, θ_l and θ_t remain finite, as the ULI constraint is not enforced in the general solution. Two components, ϕ_l and ψ_l, become inactive in a two-dimensional impact. Those components must respect the impact conditions of vanishing first and second time derivatives. This is explicitly demonstrated in Fig. 6 by plotting the derivatives for $t \in (0, t_s)$. While the velocities and accelerations of ϕ_l and ψ_l vanish at the impact, their jerks remain finite [8].

In the inset of Fig. 7, we plotted the swing foot trajectory to illustrate that no ground penetration or scuffing occurs in the swing phase. Let $\rho(t)$ be the minimal friction coefficient
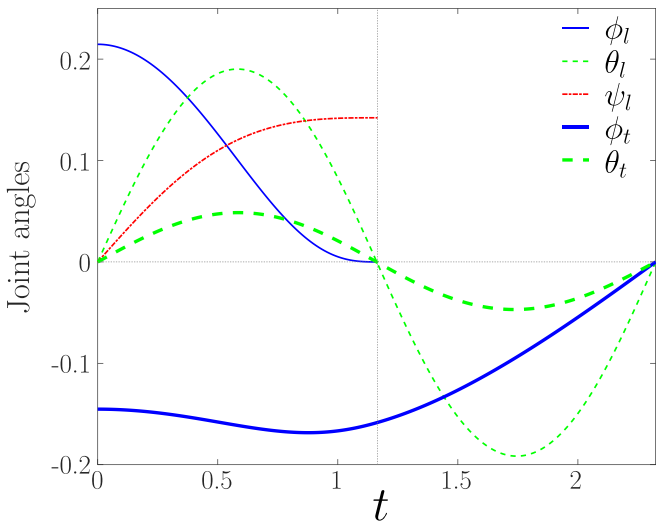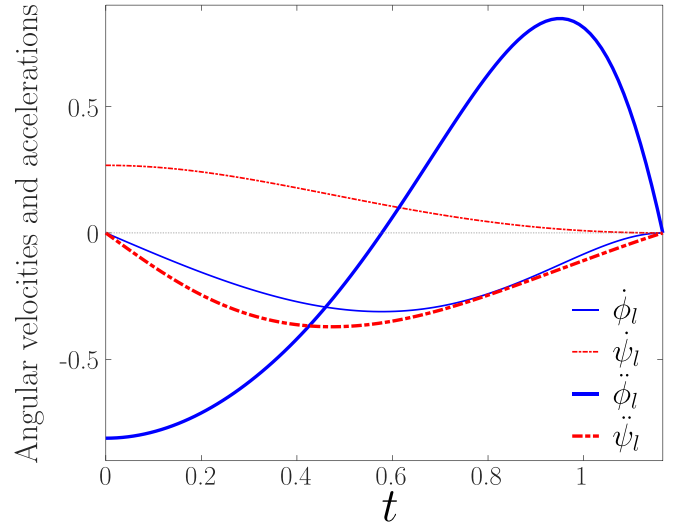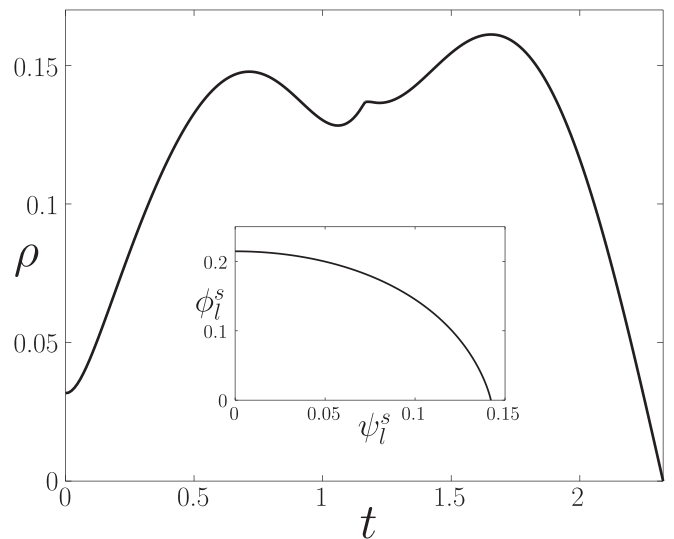

FIG. 5. Collisionless trajectory components are plotted between P_s and P_d with the following nomenclature: solid (blue), dashed (green), and dash-dotted (red) lines represent the ϕ, θ, and ψ sectors, respectively, while q_l and q_t are indicated by thin and bold lines, respectively. Vertical line is the impact moment separating phases I and II. The components θ_l, ψ_l, and θ_t vanish at P_s by symmetry. The components θ_l, ϕ_t, and θ_t vanish at P_d by symmetry. Only ϕ_l vanishes at the impact.

FIG. 7. Main panel: The minimum friction coefficient $\rho(t)$, sufficient to prevent sliding, is plotted between P_s and P_d. Inset: The parametric plot of $\phi_l(t)$ vs $\psi_l(t)$ for $t \in (0, t_s)$ shows the swing foot trajectory. The finite slope at the impact indicates finite $\rho(t_s)$.

sufficient to prevent foot sliding at time t (see also Appendix I). The finite angle of the trajectory at the impact [equal to $\mathrm{atan2}(\dddot{\phi}_l(t_s), \dddot{\psi}_l(t_s))$] implies a finite angle of the foot strike with the ground, indicating finite $\rho(t_s)$. The main panel of Fig. 7 shows $\rho(t)$ reaching maximum value of about 0.161 in phase II. Note the forces are continuous across the impact due to the enforcement of the impact conditions while the jerks are not, as manifested by a kink in $\rho(t)$ at t_s. We have verified that the ground reaction force remains non-negative throughout the cycle, thus confirming that the computed collisionless gait represents conventional walking.

The gait features the step length of about 0.085, which is 7.7% of the model height or 27.4% of the feet separation. This may seem not a lot for a normal walking, but given overall simplicity of the model and fixed feet separation, it does not look too little either. We can liken it to a penguin walk, whose feet's range is also somewhat restricted (in comparison to many bipedal animals) and whose wobbling walk also involves significant torso movements.

VII. RELATED WORK AND DISCUSSION

The optimization of a robot's design and control policies for energy efficiency is ubiquitous in the field of legged locomotion. Yet relatively few studies have addressed the possibility of complete elimination of the ground collision losses in passive walkers, even though it offers obvious benefits of greatly (indefinitely, barring the joint and air friction) extending the walking range of a robot. While the current record-holding robot [2] has narrow specialization, there is no fundamental reason for why an extreme walking efficiency and practical versatility should be mutually exclusive in robots.

The impact conditions that need to be satisfied by a collisionless conventional walking trajectory were formulated in Refs. [7,8]. The actual models chosen for the collisionless motion demonstration had relied in their design on springs. We do not view it as a critical feature, as oscillating motion can be realized by hanging pendulum-like parts as well. Springs do offer more freedom in the selection of the model's geometry, however. For example, they can be added to prop up the torso above the hip, perhaps to give the robot a more presentable look. Indeed, in Sec. V F we extended our design to include hip springs and showed that this modification only affects the parametrization of the model but not the universal aspects, such as the shape of κ_i. Ultimately, we believe the springs are only strictly necessary for propping up a single-link torso, as they enable an oscillatory mode of the standing torso, which is needed for the collision cancellation. Most likely, the same effect can be achieved by attaching the second link (e.g., a hanging arm) at the top of the standing torso.

A planar three-link biped model with a spring-mounted torso, potentially capable of collisionless walking, was proposed in Ref. [19]. It was hypothesized that, with a torso, the model had sufficient number of internal degrees of freedom to eliminate collisional losses. A version of this model, with each leg connected to the torso by a torsional spring, was solved numerically in Ref. [11], (also in Ref. [20], with an arm added to the torso). However, that solution does not enforce the acceleration vanishing at foot impacts, and therefore does not represent conventional walking. Without an additional mechanism, the walker would not be able to follow the calculated trajectory, as it would be losing its contact with the ground upon a foot strike.

The symmetry points P_s and P_d can be viewed as a generalization of the planar symmetry points imposed in Ref. [11]. There, an additional constraint of instantaneous support transfer was introduced, corresponding to $t_d \to 0$ (the impact merging with P_d) in our terminology. It turns out this constraint is incompatible with the existence of a collisionless (conventional) walking solution[1]. The double support phase appears to be necessary for realizing collisionless walking, as was originally suggested in Ref. [19].

In Sec. IV, we presented a general counting argument for the number of model parameters n that need to be tuned to realize a collisionless motion: n is one less than the impact dimension. It explains in a unified manner why $n = 0$ for the hopper [8] and the (extended) rimless wheel [9], while $n = 1$ for the three-link walker and our model. Note n does not depend directly on the number of model degrees of freedom or spatial dimensions. "Tuning" refers to a small adjustment in the vicinity of a valid solution. It does not mean that nine remaining (dimensionless) model parameters can assume arbitrary values. Still, in the SML, we were able to explicitly parametrize a wide range of admissible model parameters by means of a set of universal functions of reduced impact time (an independent nonmodel parameter) and five independent model parameters with clear restrictions on them. We find it somewhat remarkable and credit the imposition of the ULI constraint for that.

Our main contribution in this paper is the analytical analysis of a collisionless walking solution of a three-dimensional bipedal model in the SML, aided by the upright legs constraint at the impact. Similar amplitude smallness considerations have been applied to passive walking analysis on small or vanishing slopes [13,19,21], but not in the context of complete elimination of collisions, as far as we know. We consider it intuitively plausible that the SML collisionless spectrum is representative of the general collisionless modes in sufficiently large vicinity of the SML. In the same vein as the linear normal modes are representative of the nonlinear normal modes in conservative systems, under certain conditions [22]. However, we do not attempt to rigorously defend this idea. Instead, we empirically demonstrate the validity of such reasoning by numerically extending the (3,4) mode to nonsmall feet separation.

Our analysis implies that, in general, $k_\phi \geqslant 3$, and the (3,4) mode is the simplest mode under the ULI constraint. Whether an even simpler mode—(3,2) mode—exists in the absence of the constraint is an open question. We think the SML-like analysis of collisionless solution looks promising for other models, potentially more complex and more anthropomorphic models. It would be interesting to apply it to the planar three-link model. Particularly, it would be interesting to see if the problem separates into a universal part (like our equations on the impact phases) and a parametrization part, or if one needs to introduce additional constraints to make the problem

―――――――

[1]Private communication with Andy Ruina and Mario Gomes.

more tractable. It would also be interesting to consider a three-dimensional three-link model with a pelvis and spring supported torso, similar to the model introduced in Ref. [23]. To establish a walking SML solution, it would be sufficient to consider linear dynamics in the decoupled sagittal and coronal planes (with the sagittal plane dynamics identical to that of the planar three-link model). We conjecture that this model possesses collisonless walking modes, requiring two model-parameter tuning due to its three-dimensional impacts. These are just some of the possible research directions worth pursuing.

There are many ways to reduce collisional energy losses in legged locomotion, for example, via use of light-weight legs or tendonlike springs [24]. Yet, only the elimination of collisions themselves can completely eliminate collisional losses. This work extends our theoretical understanding of the related ideas and could improve the design of efficient walking robots.

APPENDIX A: ROTATION MATRIX PARAMETRIZATION

The rotations around the axes X, Y, and Z by an angle α are defined as

$$R_X(\alpha) = \begin{bmatrix} 1 & 0 & 0 \\ 0 & c & -s \\ 0 & s & c \end{bmatrix}, \quad R_Y(\alpha) = \begin{bmatrix} c & 0 & s \\ 0 & 1 & 0 \\ -s & 0 & c \end{bmatrix},$$

$$R_Z(\alpha) = \begin{bmatrix} c & -s & 0 \\ s & c & 0 \\ 0 & 0 & 1 \end{bmatrix}, \tag{A1}$$

where we have defined $c = \cos\alpha$ and $s = \sin\alpha$. Let $R_{A_i A_{i+1} \ldots A_j}(\alpha_i, \alpha_{i+1}, \ldots, \alpha_j)$ be a sequence of intrinsic (i.e., relative to the body-fixed frame) rotations, where the $(k+1)$th rotation is taken around the body axis $A_{i+k} \in \{X, Y, Z\}$ by the angle α_{i+k}:

$$R_{A_i A_{i+1} \ldots A_j}(\alpha_i, \alpha_{i+1}, \ldots, \alpha_j) = R_{A_i}(\alpha_i) R_{A_{i+1}}(\alpha_{i+1}) \ldots R_{A_j}(\alpha_j). \tag{A2}$$

We will also use shorthand notations $R_i = R_{A_i}(\alpha_i)$ and $R_{i:j}$, defined as

$$R_{i:j} = \begin{cases} i \leqslant j: & R_i R_{i+1} \ldots R_j \\ i = j+1: & I \\ i > j+1: & \text{undefined.} \end{cases} \tag{A3}$$

Assume now that $q_\alpha \equiv [\alpha_i, \alpha_{i+1}, \ldots, \alpha_j]^\mathsf{T}$ is a function of time. Let $\hat{\omega}_i = \dot{R}_i R_i^\mathsf{T}$ and $\hat{\omega}_{i:j} = \dot{R}_{i:j} R_{i:j}^\mathsf{T}$. It is straightforward to ver-

ify, for $i < j$,

$$\hat{\omega}_{i:j} = \sum_{k=i}^{k=j} R_{i:k-1} \hat{\omega}_k R_{i:k-1}^\mathsf{T} = \sum_{k=i}^{k=j} \widehat{R_{i:k-1} \omega_k}, \tag{A4}$$

which implies $\omega_{i:j} = \sum_{k=i}^{k=j} R_{i:k-1} \omega_k$. One can check that $\omega_i = I_{(\cdot f(A_i))} \dot{\alpha}_i$, where $f(A)$ maps $X \to 1$, $Y \to 2$, and $Z \to 3$. Let $R_{i:j} = R_{ab}$ be a rotation that takes F_a to F_b. Then $\omega_{i:j}$ is the angular velocity of F_b relative to F_a. Let us define S_{ab} to be a transformation relating the generalized coordinate velocity $\dot{q}_\alpha$ to the angular velocity $\omega_{i:j}$, that is, $\omega_{i:j} = S_{ab} \dot{q}_\alpha$. We then find

$$S_{ab} = [I_{(\cdot f(A_i))}, R_{i(\cdot f(A_{i+1}))}, R_{i:i+1(\cdot f(A_{i+2}))}, \ldots R_{i:k-1(\cdot f(A_k))}] \tag{A5}$$

Note the order of columns in S_{ab} follows the order of components in q_α, (as indicated by A's and α's subscripts). In the context of rotation sequences, we will refer to $R_{i:k}$ for $k < j$ as partial rotations. Thus, the matrix S_{ab} is specified in terms of the partial rotations.

The angular velocity $\omega_{i:j}$ in Eq. (A4) is specified in F_a. To transform $\dot{q}_\alpha$ to another F_c, we include a rotation R_{ca}: $\omega_{i:j}^c = R_{ca} \omega_{i:j} = S_{ab}^c \dot{q}_\alpha$, where we have defined $S_{ab}^c \equiv R_{ca} S_{ab}$. To avoid confusion, we never omit the superscript for the angular velocity transformation S_{ab}^c, unless $c = a$. We use the following shortcut notations in the paper: $S_1 \equiv S_{gl}$, $S_t \equiv S_{lt}$, $S_1^a \equiv S_{gl}^a$, and $S_t^a \equiv S_{lt}^a$.

In our model, the (fictitious) contact joint parametrization is chosen so $R_1 = R_{ZYX}(\psi_l, \theta_l, \phi_l)$. The hip joint geometry is chosen so $R_t = R_{YX}(\theta_t, \phi_t)$. Using Eq. (A5) and paying attention to the order of joint angles in q_l and q_t, we can write down the expressions for the generalized velocity transformations S_1 and S_t corresponding to R_1 and R_t, as given in Eqs. (7) and (8).

APPENDIX B: DERIVATION OF EXACT EQUATIONS OF MOTION

In this Appendix, we derive the representation of the mass matrix H and the potential term V in terms of the model constants and the joint rotations, as given in Sec. III A.

We use shortcut notations $R_1 \equiv R_{gl}$, $R_2 \equiv R_{gt}$, $R_t \equiv R_{lt}$, $\Omega_1 \equiv \Omega_{gl}$, $\Omega_2 \equiv \Omega_{gt}$, and $\Omega_t \equiv \Omega_{lt}$. We call R_1, R_t, Ω_1, and Ω_t joint rotations and angular velocities. Clearly, $\Omega_2 = \Omega_1 + \Omega_t$. Since $v_i = \dot{r}_i$, $\dot{r}_1 = \hat{\Omega}_1 r_1$, $\dot{r}_h = \hat{\Omega}_1 r_h$, $\dot{r}_t = \hat{\Omega}_2 r_t$, and $r_2 = r_h + r_t$, we have

$$\begin{aligned} v_1 &= \hat{\Omega}_1 r_1, \\ v_2 &= \hat{\Omega}_1 r_2 + \hat{\Omega}_t r_t. \end{aligned} \tag{B1}$$

We can now write the kinetic energy [see Eqs. (3)] in the basis of joint angular velocities $\Omega' = [\Omega_1; \Omega_t]$ as $T = \frac{1}{2} \Omega'^\mathsf{T} H' \Omega'$, where

$$H' = \begin{bmatrix} m_1 \hat{r}_1^\mathsf{T} \hat{r}_1 + m_2 \hat{r}_2^\mathsf{T} \hat{r}_2 + I_1 + I_2 & m_2 \hat{r}_2^\mathsf{T} \hat{r}_t + I_2 \\ m_2 \hat{r}_t^\mathsf{T} \hat{r}_2 + I_2 & m_2 \hat{r}_t^\mathsf{T} \hat{r}_t + I_2 \end{bmatrix}. \tag{B2}$$

Let us express Ω' in terms of $\dot{q}$. According to Appendix A, $\Omega_1^g = S_{gl}^g \dot{q}_l = S_1 \dot{q}_l$ and $\Omega_t^g = S_{lt}^g \dot{q}_t = R_1 S_t \dot{q}_t$. Therefore $\Omega' = S' \dot{q}$, where

$$S' = \begin{bmatrix} S_1 & 0 \\ 0 & R_1 S_t \end{bmatrix}. \tag{B3}$$

Let us rotate H' partwise so the corresponding parts' moments of inertia are diagonal in the new basis. In other words, we write $H' = R'\bar{H}R'^{\mathsf{T}}$, where

$$R' = \begin{bmatrix} R_1 & 0 \\ 0 & R_2 \end{bmatrix}. \tag{B4}$$

To compute $\bar{H} = R'^{\mathsf{T}}H'R'$, we use $r_1^g = R_1 r_1^l$, $r_2^g = R_1 r_h^l + R_2 r_t^t$, $I_1^g = R_1 I_1^l R_1^{\mathsf{T}}$, $I_2^g = R_2 I_2^l R_2^{\mathsf{T}}$, and $R_2 = R_1 R_t$ to find $\bar{H}$ given in Eqs. (9) and (10). Note that $\bar{H}$ depends only on the model constants and R_t. We can now write $T = \frac{1}{2}\Omega'^{\mathsf{T}}H'\Omega' = \frac{1}{2}\dot{q}^{\mathsf{T}}\bar{S}^{\mathsf{T}}\bar{H}\bar{S}\dot{q} = \frac{1}{2}\dot{q}^{\mathsf{T}}H\dot{q}$ where $\bar{S} = R'^{\mathsf{T}}S'$ is given in Eq. (6). The expression for V in Eq. (13) should be obvious now.

APPENDIX C: LINEAR DYNAMICS APPROXIMATION

In the linear dynamics limit, one retains all the terms up to order $O(q)$ in the equations of motion Eq. (15). This implies that the mass matrix H and the Coriolis term C must be considered up to order $O(1)$, and the potential term G up to order $O(q)$. The Coriolis term vanishes at this level, as clear from its definition in Eq. (11). We consider H and G below. Note, the derived expressions are exact to all orders in d. In this Appendix, below we refer to the quantities H, R_1, R_t, S_1, S_t, $\bar{S}$, V and G that are defined or used in Eqs. (5)–(10) and Eqs. (13) and (14).

1. Mass matrix H in linear dynamics approximation

We need to compute H to order $O(1)$ in q. To that order, $R_1 = R_t = S_1 = I$, $S_t = I_{3\times 2}$ and $\bar{S} = [I_{3\times 3}, 0; 0, I_{3\times 2}]$. Using Eqs. (1) and (I1) to compute products of the form $\hat{r}^{\mathsf{T}}\hat{r}'$ in Eqs. (10), one readily arrives at the expressions below.

In the linear dynamics limit $H \to H_0 = [H_{ll}^0, H_{lt}^0; H_{tl}^0, H_{tt}^0]$, where

$$H_{ll}^0 = \begin{bmatrix} \mu_2 + I_\phi + \mu_0 d^2 & 0 & 0 \\ 0 & \mu_2 + I_\theta & -\mu_1 d \\ 0 & -\mu_1 d & I_\psi + \mu_0 d^2 \end{bmatrix},$$

$$H_{tl}^0 = \begin{bmatrix} -m_2 l_2 l_t + I_{2\phi} & 0 & 0 \\ 0 & -m_2 l_2 l_t + I_{2\theta} & m_2 l_t d \end{bmatrix},$$

$$H_{tt}^0 = \begin{bmatrix} m_2 l_t^2 + I_{2\phi} & 0 \\ 0 & m_2 l_t^2 + I_{2\theta} \end{bmatrix}, \tag{C1}$$

and $H_{lt}^0 = H_{tl}^{0\mathsf{T}}$.

2. Potential term G in linear dynamics approximation

To compute G to order $O(q)$, we need to compute the potential energy V, and hence the joint rotation matrices R_1 and R_t [see Eq. (13)], to order $O(q^2)$. To quadratic order, we find

$$R_1 = R_{ZYX}(\psi, \theta, \phi)$$
$$= \begin{bmatrix} 1 - \frac{\theta^2 + \psi^2}{2} & -\psi & \theta \\ \psi & 1 - \frac{\phi^2 + \psi^2}{2} & -\phi \\ -\theta & \phi & 1 - \frac{\phi^2 + \theta^2}{2} \end{bmatrix} \tag{C2}$$

and

$$R_t = R_{YX}(\theta, \phi) = \begin{bmatrix} 1 - \frac{\theta^2}{2} & \phi\theta & \theta \\ 0 & 1 - \frac{\phi^2}{2} & -\phi \\ -\theta & \phi & 1 - \frac{\phi^2 + \theta^2}{2} \end{bmatrix}. \tag{C3}$$

From Eq. (13), we find to quadratic order:

$$V = \mu_1 + \mu_0 d\phi_l - \mu_1 \frac{\phi_l^2 + \theta_l^2}{2}$$
$$+ m_2 l_t \left(\frac{\phi_l^2 + \theta_l^2}{2} + \phi_l \phi_t + \theta_l \theta_t \right). \tag{C4}$$

For G, we find $G = G_0 + G_1 q$, where $G_0 = [g\mu_0 d, 0, 0, 0, 0]^{\mathsf{T}}$ and

$$G_1 = -g\mu_1 \begin{bmatrix} 1 & 0 & 0 & 0 & 0 \\ 0 & 1 & 0 & 0 & 0 \\ 0 & 0 & 0 & 0 & 0 \\ 0 & 0 & 0 & 0 & 0 \\ 0 & 0 & 0 & 0 & 0 \end{bmatrix}$$

$$+ gm_2 l_t \begin{bmatrix} 0 & 0 & 0 & 1 & 0 \\ 0 & 0 & 0 & 0 & 1 \\ 0 & 0 & 0 & 0 & 0 \\ 1 & 0 & 0 & 1 & 0 \\ 0 & 1 & 0 & 0 & 1 \end{bmatrix}. \tag{C5}$$

APPENDIX D: HIGHER ORDER CORRECTION TO LINEAR DYNAMICS APPROXIMATION

The next order terms on top of the linear dynamics approximation captured by Eqs. (19) come from expanding H_0 to order $O(\bar{d})$ and from expanding H and C to order $O(q)$ at $d = 0$. The latter constitutes a nonlinear correction to the linear dynamics approximation. We denote those terms $H_1(q)$ and $C_1(\dot{q})$ for the mass matrix and the Coriolis term corrections, respectively. Expanding H_0 (defined in Appendix C 1) to order $O(\bar{d})$ contributes the term $db^{\mathsf{T}}\ddot{q}_\theta$ in Eq. (20). For $H_1(q)$, one finds

$$H_1(q) = e_3 q^{\mathsf{T}} A + A^{\mathsf{T}} q e_3^{\mathsf{T}}, \tag{D1}$$

where $e_3 = [0, 0, 1, 0, 0]^{\mathsf{T}}$ and A is defined in terms of the elements $A_{\alpha\beta}^{ij} \equiv A_{\alpha\beta(ij)}$ of the matrices $A_{\phi\theta}$ and $A_{\theta\phi}$, given in Eqs. (22):

$$A = \begin{bmatrix} 0 & A_{\phi\theta}^{11} & 0 & 0 & A_{\phi\theta}^{12} \\ A_{\theta\phi}^{11} & 0 & 0 & A_{\phi\theta}^{12} & 0 \\ 0 & 0 & 0 & 0 & 0 \\ 0 & A_{\phi\theta}^{21} & 0 & 0 & A_{\phi\theta}^{22} \\ A_{\theta\phi}^{21} & 0 & 0 & A_{\theta\phi}^{22} & 0 \end{bmatrix}. \tag{D2}$$

The term $C_1(\dot{q})$ is determined by $H_1(q)$ via Eqs. (11) and (12). We find

$$\frac{\partial H_1(q)}{\partial q_{(k)}} = e_3 A_{(k\cdot)} + (A^{\mathsf{T}})_{(\cdot k)} e_3^{\mathsf{T}}, \tag{D3}$$

the Christoffel symbols

$$\Gamma^k = \frac{1}{2}(e_3(A + A^{\mathsf{T}})_{(k\cdot)} - (A - A^{\mathsf{T}})_{(\cdot k)} e_3^{\mathsf{T}} - (A - A^{\mathsf{T}})e_{3(k)}), \tag{D4}$$

and the Coriolis term

$$
C_1(\dot{q}) = \tfrac{1}{2}\big(e_3\dot{q}^\mathsf{T}(A + A^\mathsf{T}) - (A - A^\mathsf{T})(\dot{q}e_3^\mathsf{T} + e_3^\mathsf{T}\dot{q}I_{5\times5})\big).
$$
(D5)

The corresponding contribution to the equations of motion Eq. (20) in the ψ sector is

$$
\begin{aligned}
e_3^\mathsf{T}(H_1(q)\ddot{q} + C_1(\dot{q})\dot{q}) &= q^\mathsf{T}A\ddot{q} + \frac{1}{2}\dot{q}^\mathsf{T}(A + A^\mathsf{T})\dot{q} \\
&= \frac{d}{dt}(q^\mathsf{T}A\dot{q}) \\
&= \frac{d}{dt}\big(q_\phi^\mathsf{T}A_{\phi\theta}\dot{q}_\theta + q_\theta^\mathsf{T}A_{\theta\phi}\dot{q}_\phi\big).
\end{aligned}
$$
(D6)

APPENDIX E: CORONAL SECTOR IMPACT TIME EQUATIONS

To reduce clutter, we omit the coronal sector superscript ϕ in this section. The last four equations in Eqs. (52) form a homogeneous linear system $Aw = 0$, where

$$
A = \begin{bmatrix}
u_{+(1)}^s\omega_+^s s_+^s & u_{-(1)}^s\omega_-^s s_-^s & 0 \\
u_{+(1)}^s\omega_+^{s\,2} c_+^s & -u_{-(1)}^s\omega_-^{s\,2} c_-^s & 0 \\
u_{+(2)}^s c_+^s & u_{-(2)}^s c_-^s & s^d \\
u_{+(2)}^s\omega_+^s s_+^s & u_{-(2)}^s\omega_-^s s_-^s & -\omega^d c^d
\end{bmatrix},
$$
(E1)

where we have defined $c_z^s = \cosh\sqrt{z}\omega_z^s t_s$, $s_z^s = \sqrt{z}\sinh\sqrt{z}\omega_z^s t_s$, $c^d = \cos\omega^d t_d$, and $s^d = \sin\omega^d t_d$.

Consider the task of reducing the rank of a $n \times m$ matrix M, with $n > m$, below m. To achieve it, one needs to tune at least $n - m + 1$ parameters of M, in general. Indeed, for A this can be done by tuning two parameters, t_s and t_d.

Consider two submatrices of A: (1) a 2×2 matrix A_1, which is the top left corner submatrix of A, and (2) a 3×3 matrix A_2, which is obtained from A by dropping the second row. If A_1 and A_2 are singular matrices, then A has rank at most 2. One can see it as follows. The singularity of A_1 implies that the rows $A_{(1\cdot)}$ and $A_{(2\cdot)}$ are not independent. The singularity of A_2 implies that among $A_{(1\cdot)}$, $A_{(3\cdot)}$, and $A_{(4\cdot)}$ there are at most two independent rows. Hence A has at most two independent rows.

Let $A:A_{(i\cdot)}$ be a matrix obtained from A by the elementwise division of its rows by ith row. We first test the singularity of A_1,

$$
\det(A_1:A_{1(1\cdot)}) = \omega_-^s\cot\omega_-^s t_s - \omega_+^s\coth\omega_+^s t_s,
$$
(E2)

from where the first equation in Eqs. (53) follows.

To test the singularity of A_2, we compute

$$
\begin{aligned}
&\det(A_2:A_{2(3\cdot)}) \\
&= -\frac{\sigma_+}{\omega_-^s}\cot\omega_-^s t_s - \frac{\sigma_-}{\omega_+^s}\coth\omega_+^s t_s + \frac{\sigma_+ - \sigma_-}{\omega^d}\tan\omega^d t_d \\
&= -\left(\frac{\sigma_+}{\omega_-^{s\,2}} + \frac{\sigma_-}{\omega_+^{s\,2}}\right)\omega_-^s\cot\omega_-^s t_s + \frac{\sigma_+ - \sigma_-}{\omega^d}\tan\omega^d t_d,
\end{aligned}
$$
(E3)

where $\sigma_z = u_{z(1)}^s/u_{z(2)}^s$. In the second step, we assumed $\det A_1 = 0$ and used Eq. (E2). Next, we compute

$$
\begin{aligned}
\frac{\sigma_+ - \sigma_-}{\frac{\sigma_+}{\omega_-^{s\,2}} + \frac{\sigma_-}{\omega_+^{s\,2}}} &= \frac{\Lambda_{-,+}^\lambda - \Lambda_{-,-}^\lambda}{\Lambda_{-,-}^\lambda\Lambda_{+,+}^\lambda - \Lambda_{-,+}^\lambda\Lambda_{+,-}^\lambda} \\
&= \frac{1}{\Lambda_{-,+}^\lambda - \Lambda_{+,+}^\lambda} = \frac{1}{-a_-} = \omega^{d\,2},
\end{aligned}
$$
(E4)

where we used Eqs. (42) and (I2). From Eqs. (E3) and (E4), the second equation in Eqs. (53) follows.

APPENDIX F: MODEL PARAMETRIZATION

In this Appendix, we fill in the details omitted in Sec. V E. Our goal is to realize the impact phase solution (at a given $\bar{\tau}$) by tuning the minimal number of the model parameters. We first focus on the ϕ sector. The impact phases are completely specified by a_z^ϕ, γ and τ. Since the impact phases are defined by three frequencies, we are going to tune τ and two model parameters. To this end, we first solve for a_+^ϕ and γ, with a_-^ϕ fixed and $\tau = \bar{\tau}\sqrt{\gamma}$. Let us write Eq. (43) as $a_z^\phi = \gamma\bar{a}_{+z}^\phi = \gamma\Lambda_{+z}(\bar{\lambda}_+^\phi, \bar{\lambda}_-^\phi, 1)$. From where we get: $a_+^\phi = a_-^\phi\bar{a}_{++}^\phi/\bar{a}_{+-}^\phi$ and $\gamma^2 = a_-^{\phi\,2}(\bar{a}_{+-}^\phi)^{-2}$. Using Eqs. (I3), we find

$$
\frac{\bar{a}_{++}^\phi}{\bar{a}_{+-}^\phi} = \frac{\bar{a}_{++}^\phi\bar{a}_{+-}^\phi}{\bar{a}_{+-}^\phi\bar{a}_{+-}^\phi} = \frac{\bar{\lambda}_+^\phi\bar{\lambda}_-^\phi - 1}{(\bar{a}_{+-}^\phi)^2}.
$$
(F1)

We can now write the equations on a_+^ϕ and γ^2 in the form

$$
\begin{aligned}
a_+^\phi &= -a_-^\phi(\kappa_1^2 + 1)\kappa_2, \\
\gamma^2 &= a_-^{\phi\,2}\kappa_2,
\end{aligned}
$$
(F2)

where κ_i were defined in Eqs. (61). Let us work in dimensionless units by setting $g = m_2 = l_t = 1$. Let us also parametrize the moments of inertia as $I_{1\alpha} = c_1^\alpha\tilde{\mu}_2$ and $I_{2\alpha} = c_2^\alpha m_2 l_t^2 = c_2^\alpha$. The expressions for a_z^ϕ and γ^2, in terms of the model parameters [see Eqs. (38)], now read

$$
a_+^\phi = \frac{\tilde{\mu}_2}{\tilde{\mu}_1}(1 + c_1^\phi), \quad a_-^\phi = -(1 + c_2^\phi), \quad \gamma^2 = \frac{l_h^2}{\tilde{\mu}_1}. \quad \text{(F3)}
$$

We first consider a simpler case of $c_i^\phi = 0$. Plugging a_z^ϕ and γ^2 from Eqs. (F3) into Eqs. (F2) and solving for l_h and l_1, one readily finds Eqs. (60). We next consider the general case of $c_i^\phi > 0$. Let us express κ_i as

$$
\begin{aligned}
\kappa_1^2 + 1 &= (\kappa_1'^2 + 1)(1 + c_1^\phi)(1 + c_2^\phi), \\
\kappa_2 &= \kappa_2'(1 + c_2^\phi)^{-2}.
\end{aligned}
$$
(F4)

If we now plug a_z^ϕ and γ^2 from Eqs. (F3) and κ_i from Eqs. (F4) into Eqs. (F2), we get equations on l_h and l_1 which look exactly like the $c_i^\phi = 0$ case but with κ_i replaced by κ_i'. It follows that the general case solution must have the form of Eqs. (60) with κ_i replaced by κ_i'.

We consider the θ sector next. Let us express a_-^θ in terms of a_+^θ, λ_-^θ, and γ^2, by inverting $\lambda_-^\theta = \lambda_{+-}^\theta$, see Eqs. (42). We find

$$
a_-^\theta = \lambda_-^\theta + \frac{\gamma^2}{\lambda_-^\theta - a_+^\theta}.
$$
(F5)

Equation (50) implies $\lambda_-^\theta = -\tau^2/\pi^2$. Notice that $\tilde{\mu}_2/\tilde{\mu}_1$ and γ^2 are purely functions of κ_i': $\tilde{\mu}_2/\tilde{\mu}_1 = (\kappa_1'^2 + 1)\kappa_2'$ and $\gamma^2 = \kappa_2'$. Therefore, we can write $a_+^\theta = (\kappa_1'^2 + 1)\kappa_2'(1 + c_1^\theta)$. Plugging the above expressions for λ_-^θ, γ^2 and a_+^θ into Eq. (F5), while replacing a_-^θ with $-(1 + I_{2\theta})$, we obtain Eq. (66) and the restricted version Eq. (64).

Let us analyze the function $\Phi(\xi, \kappa_1, \kappa_2)$, implicitly introduced via Eq. (67) in Sec. V E 2. We will use the restricted solution quantities τ^r and $I_{2\theta}^r$, as indicated by the superscript r. Note, $\xi = (\tau^r/\pi)^2$. Using Eq. (64), we can cast $\Phi(\xi, \kappa_1, \kappa_2)$ in the form:

$$\Phi(\xi, \kappa_1, \kappa_2) \equiv \frac{(1 - \xi^2)^{-1} - \xi^2 \kappa_2^{-1}}{\kappa_1^2 + 1}$$
$$= 1 + I_{2\theta}^r \frac{\xi^2 \kappa_2^{-1} + \kappa_1^2 + 1}{(1 - \xi^2)(\kappa_1^2 + 1)}. \qquad \text{(F6)}$$

Since $I_{2\theta}^r$ and κ_2 are both positive, $\Phi(\xi, \kappa_1, \kappa_2) > 1$ provided $\xi < 1$.

To prove that $0 < u_{-(1)}^\theta < u_{-(2)}^\theta$, we observe that $0 < \lambda_{--} \leqslant \gamma < \gamma\beta$, since $\tilde{\mu}_1 > m_2 l_t$, see Eqs. (38). The result then follows from Eqs. (42). Also, $u_{-(2)}^\theta > \beta u_{-(1)}^\theta$.

APPENDIX G: UP-DOWN TORSO DUALITY

In the dimensionless units, H_α and $G_{1\alpha}$ are

$$H_\alpha = \begin{bmatrix} h_1 & h_z \\ h_z & h_2 \end{bmatrix}, \quad G_{1\alpha} = \begin{bmatrix} g_1 & z \\ z & z + \text{k} \end{bmatrix}, \qquad \text{(G1)}$$

where

$$h_1 = \mu_2 + I_\alpha, \quad h_2 = 1 + I_{2\alpha}, \quad h_z = z l_h + h_2,$$
$$g_1 = -\mu_1. \qquad \text{(G2)}$$

Computing $\tilde{H}_\alpha$ and $\tilde{G}_{1\alpha}$ [see Eq. (24)] with $\tilde{S}$ defined in Eq. (74) and selecting y that diagonalizes $\tilde{G}_{1\alpha}$ we find

$$\tilde{H}_\alpha = \begin{bmatrix} h_1 - 2z h_z \text{y} + h_2 \text{y}^2 & z h_z - h_2 \text{y} \\ z h_z - h_2 \text{y} & h_2 \end{bmatrix},$$
$$\tilde{G}_{1\alpha} = \begin{bmatrix} g_1 - \text{y} & 0 \\ 0 & \frac{1}{\text{y}} \end{bmatrix}, \qquad \text{(G3)}$$

where $\text{y} = 1/(z + \text{k})$. As explained in Sec. V F, we want $\tilde{H}_\alpha$ and $\tilde{G}_{1\alpha}$ to be independent of z. It then follows from Eq. (G3) that y, g_1, h_1, h_2, and $z h_z$ are all independent of z. Solving $\text{y}' = \text{y}$ and $z' h_z' = z h_z$ with $z' = -z$, where the prime denotes quantities in the dual setup, we find

$$\text{k}' = \text{k} + 2z, \quad l_h' = l_h + 2z h_2. \qquad \text{(G4)}$$

Note that $\mu_1' = \mu_1$. If we demand $I_{1\alpha}$ to be fixed, then we also have $\mu_2' = \mu_2$. From there, the transformation law for m_1 and l_1 in Eqs. (75) easily follows, where $\delta_n = m_1' l_1'^n = \mu_n - (l_h' - z')^n$. To derive a condition for $\delta_n > 0$, we use Eqs. (60) to substitute l_1 and l_h to find a quadratic equation on $\sqrt{m_1}$. Solving the quadratic equations we arrive at Eqs. (78). The condition in Eq. (80) is similarly derived from $\beta > 2 + \text{y}$, which implies x $< 1/(2 + \text{y})$.

APPENDIX H: CONSTRAINED GRADIENT DESCENT

We enforce the triangle inequality (for the moments of inertia) by setting up a one-to-one correspondence between triangle's side lengths (d_1, d_2, d_3) and a triplet (η_1, η_2, η_3) of real numbers. We require that the triangle's perimeter is $\sum_i d_i = P = \sum_i e^{\eta_i}$ and the opposing angles are $\alpha_i = \pi e^{\eta_i}/P$. One then finds for the mapping:

$$d_i = \frac{P \sin \frac{\pi e^{\eta_i}}{P}}{\sum_i \sin \frac{\pi e^{\eta_i}}{P}},$$
$$\eta_i = \ln \left(\frac{P}{\pi} \arccos \frac{\sum_{j \neq i} d_j^2 - d_i^2}{2 \Pi_{j \neq i} d_j} \right). \qquad \text{(H1)}$$

This parametrization is only suitable for enforcing the strict triangle inequality (the general case in Sec. V E 2), as $\eta_i \to -\infty$ for $d_i \to 0$.

Consider a constrained optimization problem of finding x that maximizes an objective function $f(x)$ under the constraints $\|x - x_0\| = \epsilon$ and $h(x) = 0$. Solving it amounts to finding the stationary points of the Lagrangian function

$$f(x) + \lambda_h^\mathsf{T} h(x) + \frac{\lambda_x}{2}((x - x_0)^\mathsf{T}(x - x_0) - \epsilon^\mathsf{T}\epsilon) \qquad \text{(H2)}$$

with respect to x and the Lagrange multipliers λ_h and λ_x. Assuming that x_0 approximately satisfies $h = 0$ and ϵ is small, we can optimize an approximate Lagrangian function where $f(x)$ and $h(x)$ have been replaced by their first order expansion around x_0. The result of this is Eq. (82) with implicit dependence of λ_x on ϵ, (with x_0 and x replaced by x_i and x_{i+1}). In practice, we dispense with ϵ and treat λ_x as the controlling parameter of the gradient descend rate.

APPENDIX I: MISCELLANEOUS RELATIONS AND PROPERTIES

In this Appendix, we gather an eclectic mix of relations and properties used in the paper. Product of skew symmetric matrices can be expressed via respective vectors as

$$\hat{a}^\mathsf{T} \hat{b} = (a^\mathsf{T} b)I - b a^\mathsf{T}. \qquad \text{(I1)}$$

It is easy to see that a real-valued 2×2 matrix M with $\det M < 0$ has one positive and one negative eigenvalue: the discriminant of the characteristic polynomial $\lambda^2 - \lambda \text{Tr} M + \det M$ is positive, therefore the eigenvalues are real, nonzero, and of different signs.

It is easy to verify a number of useful relations on $\Lambda_{zz'}$ using its definition in Eq. (40):

$$\Lambda_{z,z'}(a, b, c) + \Lambda_{-z,-z'}(a, b, c) = a,$$
$$\Lambda_{z,z'}(a, b, c) - \Lambda_{-z,z'}(a, b, c) = zb, \qquad \text{(I2)}$$

and

$$\Lambda_{-+}(a, b, c)\Lambda_{--}(a, b, c) = -c,$$
$$\Lambda_{++}(a, b, c)\Lambda_{+-}(a, b, c) = ab - c. \qquad \text{(I3)}$$

To prove Eq. (54) relating the coronal sector frequencies, we compute

$$(a_- - \lambda_-)(a_- - \lambda_+) = \lambda_{--}\lambda_{-+} = \gamma^2, \qquad \text{(I4)}$$

where we used Eqs. (41), (42), (I2), and (I3).

The values of χ, that is, the initial conditions on q^p and t_p, fully specifying (in addition to the model parameters η) the (3,4) mode, numerically studied in Sec. VI, are given below:

$$\phi_l^s = 0.2146047,$$
$$\phi_t^s = -0.1452115,$$
$$\dot{\theta}_l^s = 0.5255085,$$
$$\dot{\psi}_l^s = 0.2670555,$$
$$\dot{\theta}_t^s = 0.1306085$$
$$\dot{\theta}_l^d = 0.5369450,$$

$$\dot{\phi}_t^d = 0.1716506,$$
$$\dot{\theta}_t^d = 0.1257789,$$
$$t_s = 1.1657382,$$
$$t_d = 1.1582562. \qquad \text{(I5)}$$

It is straightforward to compute the minimum friction coefficient ρ given the moment of gravity force $M_g = \sum_i m_i \hat{r}_i g_f$, the momentum $P = \sum_i m_i v_i$, and the angular momentum $L = \partial \mathcal{L} / \partial \Omega_1$ [16]. One readily finds $M_g = R_1(m_1 \hat{r}_1^l + m_2 \hat{r}_2^l) g_f$ and $P = R_1[m_1 \hat{r}_1^l + m_2 \hat{r}_2^l; m_2 \hat{r}_t^t R_t^\mathsf{T}]^\mathsf{T} \bar{S} \dot{q}$, where $r_2^l = r_h^l + R_t r_t^t$. It is also easy to find $L = R_1(\bar{H} \bar{S} \dot{q})_{(l)}$, see the last paragraph of Appendix B.

[1] D. C. Post, Robustness and efficiency of planar biped walking robots, Ph.D. thesis, University of Notre Dame, 2013.

[2] P. A. Bhounsule, J. Cortell, A. Grewal, B. Hendriksen, J. G. D. Karssen, C. Paul, and A. Ruina, Low-bandwidth reflex-based control for lower power walking: 65 km on a single battery charge, Int. J. Robotics Res. **33**, 1305 (2014).

[3] R. M. Alexander, Optimization and gaits in the locomotion of vertebrates, Physiol. Rev. **69**, 1199 (1989).

[4] F. C. Anderson and M. G. Pandy, Dynamic optimization of human walking, J. Biomech. Eng. **123**, 381 (2001).

[5] T. McGeer, Passive dynamic walking, I. J. Robotic Res. **9**, 62 (1990).

[6] S. H. Collins, M. Wisse, and A. Ruina, A three-dimensional passive-dynamic walking robot with two legs and knees, Int. J. Robotics Res. **20**, 607 (2001).

[7] C. K. Reddy and R. Pratap, A passive hopper with lossless collisions, in *IUTAM Symposium on Nonlinearity and Stochastic Structural Dynamics*, edited by S .Narayanan and R. N. Iyengar, Solid Mechanics and its Applications Vol. 85 (Springer, Dordrecht, 2001), pp. 209–220.

[8] A. Chatterjee, R. Pratap, C. K. Reddy, and A. Ruina, Persistent passive hopping and juggling is possible even with plastic collisions, Int. J. Robotics Rese. **21**, 621 (2002).

[9] M. W. Gomes, Collisionless rigid body locomotion models and physically based homotopy methods for finding periodic motions in high degree of freedom models, Ph.D. thesis, Cornell University, Department of Theoretical and Applied Mechanics, 2005.

[10] M. W. Gomes and K. Ahlin, Quiet (nearly collisionless) robotic walking, in *2015 IEEE International Conference on Robotics and Automation (ICRA)* (IEEE, Seattle, WA, USA, 2015), pp. 5761–5766.

[11] M. Gomes and A. Ruina, Walking model with no energy cost, Phys. Rev. E **83**, 032901 (2011).

[12] M. W. Gomes and A. L. Ruina, A five-link 2d brachiating ape model with life-like zero-energy-cost motions, J. Theor. Biol. **237**, 265 (2005).

[13] M. Garcia, A. Chatterjee, and A. Ruina, Efficiency, speed, and scaling of two-dimensional passive-dynamic walking, Dyn. Stability Syst. **15**, 75 (2000).

[14] K. Trifonov and S. Hashimoto, Active knee-lock release for passive-dynamic walking machines, in *IEEE International Conference on Robotics and Biomimetics*, ROBIO 2007 (IEEE, Sanya, China, 2007), pp. 958–963.

[15] T. McGeer, Passive walking with knees, in *Proceedings., IEEE International Conference on Robotics and Automation* (IEEE, Cincinnati, OH, USA, 1990), pp. 1640–1645.

[16] L. D. Landau and E. M. Lifshitz, *Mechanics*, Course of Theoretical Physics Series Vol. 1 (Oxford Pergamon Press, Oxford, 2000).

[17] R. M. Murray, Z. Li, and S. S. Sastry, *A Mathematical Introduction to Robotic Manipulation* (CRC Press, Boca Raton, FL, 1994).

[18] J. W. Eaton, D. Bateman, S. Hauberg, and R. Wehbring, *GNU Octave Version 4.2.1 Manual: A High-Level Interactive Language for Numerical Computations* (2017), https://www.gnu.org/software/octave/doc/v4.2.1/.

[19] A. Chatterjee and M. Garcia, Small slope implies low speed for McGeer's passive walking machines, Dyn. Stability Syst. **15**, 139 (2000).

[20] T. Chyou, G. F. Liddell, and M. G. Paulin, An upper-body can improve the stability and efficiency of passive dynamic walking, J. Theor. Biol. **285**, 126 (2011).

[21] M. Garcia, A. Chatterjee, A. Ruina, and M. J. Coleman, The simplest walking model: stability, complexity, and scaling, J. Biomech. Eng. **120**, 281 (1998).

[22] A. M. Lyapunov, The general problem of the stability of motion, Int. J. Control **55**, 531 (1992).

[23] S. Faraji and A. J. Ijspeert, 3LP: A linear 3D-walking model including torso and swing dynamics, Int. J. Robotics Res. **36**, 436 (2017).

[24] M. Srinivasan, Fifteen observations on the structure of energy-minimizing gaits in many simple biped models, J. R. Soc. Interface **8**, 74 (2011).